NEANDC (E)-272 U Vol. V
INDC (Ger)-29/LN + Special

PROGRESS REPORT ON NUCLEAR DATA RESEARCH IN THE FEDERAL REPUBLIC OF GERMANY

for the Period April 1, 1985 to March 31, 1986

June 1986

Edited by
S. M. Qaim

Institut für Chemie (1): Nuklearchemie
Kernforschungsanlage Jülich GmbH

NEANDC (E)-272 U Vol. V
INDC (Ger)-29/LN + Special

PROGRESS REPORT ON NUCLEAR DATA RESEARCH IN THE FEDERAL REPUBLIC OF GERMANY

for the Period April 1, 1985 to March 31, 1986

June 1986

Edited by
S. M. Qaim

Institut für Chemie (1): Nuklearchemie
Kernforschungsanlage Jülich GmbH

F O R E W O R D

This report has been prepared to promote exchange of nuclear data research information between the Federal Republic of Germany and other member states of NEA and IAEA. It brings together progress reports from KfK Karlsruhe, KFA Jülich, GKSS-Geesthacht, the Universities of Kiel, Hamburg, Köln, Mainz, Marburg, Stuttgart and München, as well as from PTB Braunschweig und FIZ Karlsruhe. As in previous years, the emphasis in the work reported here has been on measurement, evaluation and compilation of application oriented nuclear data, such as those relevant to fission and fusion reactor technologies, development of intense spallation neutron sources, astrophysics research, cosmogenic and meteoritic investigations, production of medically important short-lived radioisotopes, etc.

Each contribution is presented under the laboratory heading where the work was done. If the work is relevant to requests in the World Request List for Nuclear Data, WRENDA 83/84 (INDC(SEC)-88/URSF), the corresponding request identification numbers have been listed after the title and authors' names of the respective contribution.

Jülich, June 1986 S.M. Qaim

C O N T E N T S

Page

REAKTORSTATION GARCHING

FACHBEREICH PHYSIK

TECHNISCHE UNIVERSITÄT MÜNCHEN

Page

KERNFORSCHUNGSZENTRUM KARLSRUHE
INSTITUT FÜR KERNPHYSIK II

1. Validation of HETC Model Calculations for Proton-Induced Neutron Production

S. Cierjacks, Y. Hino[1], D. Filges[2], T.W. Armstrong[2], P. Cloth[2]

The previous studies to assess the accuracy of intranuclear cascade-evaporation model predictions for neutron production from high-energy proton bombardment have been continued. For this purpose model calculations employing the HETC/KFA-1 code [1] were compared with the systematic KfK measurements at 585 MeV proton energy [2]. These comparisons showed that the code can satisfactorily reproduce the measured double differential neutron production cross sections in the evaporation region for medium and heavy weight nuclei. The evaporation model is, however, inadequate for the two lightest nuclei, aluminum and carbon. Neutron production from the intranuclear cascade differs from experimental measurements by large factors. This is illustrated in Fig. 1 which shows the ratio of calculated to measured cross sections versus energy for tantalum. While the 30°-data differ only strongly in the intermediate region between about 50 and 300 MeV, the largest discrepancies occur in the 90°- and 150°-data at the upper ends of the two spectra. This behavior is similar for all other target elements studied. A closer inspection of the large differences shows that these occur in spectral regions in which neutron production associated with quasifree pion production is expected to be dominant [3]. This seems to indicate that the models for pion-nucleon interactions used in the HETC code are insufficient. Thus, a re-evaluation of pion-nucleon cross sections from contemporary experimental data is planned [4].

2. Nuclear Data Needs for Intense Neutron Sources

S. Cierjacks

Nuclear data needs for the design and operation of new intense neutron sources have been surveyed in an invited paper [5]. Some advanced sources have recently been put into operation, and others are under construction or under study for use in radiotherapy, fusion technology and condensed matter research. For application in these fields the most appropriate types are 14 MeV DT, deuteron break-up and spallation neutron sources. Nuclear data aspects related to the proper and

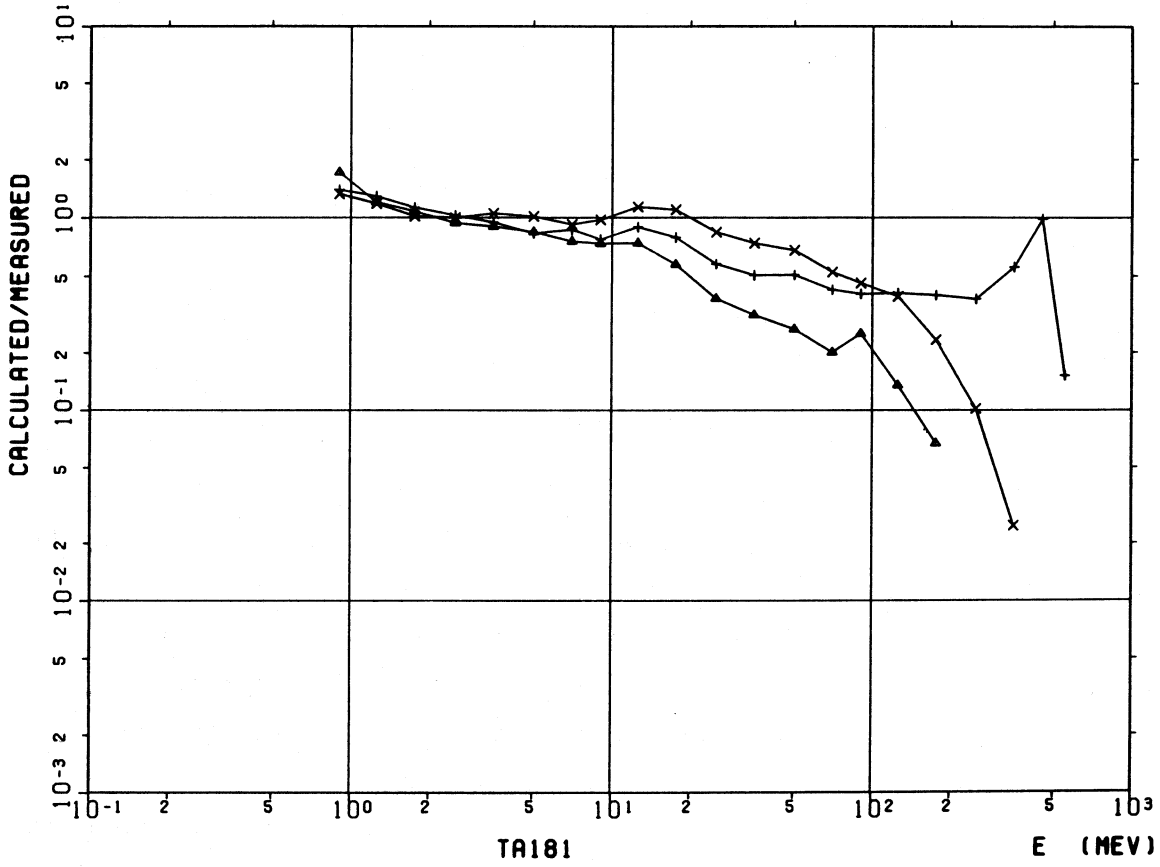

Fig. 1. Ratios of calculated to measured neutron production cross sections versus energy for Ta. The three curves refer to data at emission angles of 30° (+), 90° (x) and 150° (▲).

economic design and operation of such sources have been discussed for four main areas of interest: 1. Predictions and determinations of source properties. 2. Performance of source and accelerator shielding. 3. Study of safety and maintenance problems. 4. Performance of neutron dosimetry and determination of radiation damage parameters. Considering nuclear data involved in these areas of interest, existing data from evaluated files, recent measurements and model calculations were critically examined. Remaining nuclear data needs were then identified on this basis. There is a clear need of more precise nuclear data for many technologically important materials in the extended energy region from about a few MeV up to 1 GeV. In this range very few measurements have been made, and there is little prospect for a drastic change of this situation. Therefore, the majority of lacking data must come from nuclear model calculations. Existing nuclear model codes need, however, verification from comparisons with contemporary experimental results, before reliable results can be obtained in the extended mass and energy regions.

3. High-Resolution Studies with a Large-Area Position-Sensitive Time-of-Flight Counter

S. Cierjacks, S. Ljungfelt, H. Ullrich, T. Petkovič[3], N. Šimičevič[3], H.J. Weyer[4]

Time and position resolutions of a large time-of-flight counter developed for neutron and charged-particle detection in the energy range from 10 to 300 MeV have been studied [6]. The counter consists of thirty plastic scintillator bars (NE 102A) of 5 x 10 cm^2 cross section and 2 m length. The bars are arranged in a suitable counter matrix to give an overall effective detection area of 1 x 2 m^2. The whole set of counter bars is grouped into five modules consisting of six bars each with two layers of bars in height and three in depth. In front of each module a common anticounter (a 0.4 cm thick plastic scintillator) is used to allow identification of events from neutrons and charged particles. The individual main counter bars have pulse-height responses over the length uniform to 5% except close to the ends. Typical integral neutron detection efficiencies are 19% at 50 MeV and 13% at 170 MeV for a pulse-height threshold of 5 MeV electron-equivalent energy. A typical measurement of the time resolution is shown in Fig. 2. It can be seen that the intrinsic time dispersion of a main counter bar is 450 ps when XP-2020 photomultipliers are used. This results in a position resolution of almost 5 cm and a position-independent energy resolution of 3% at

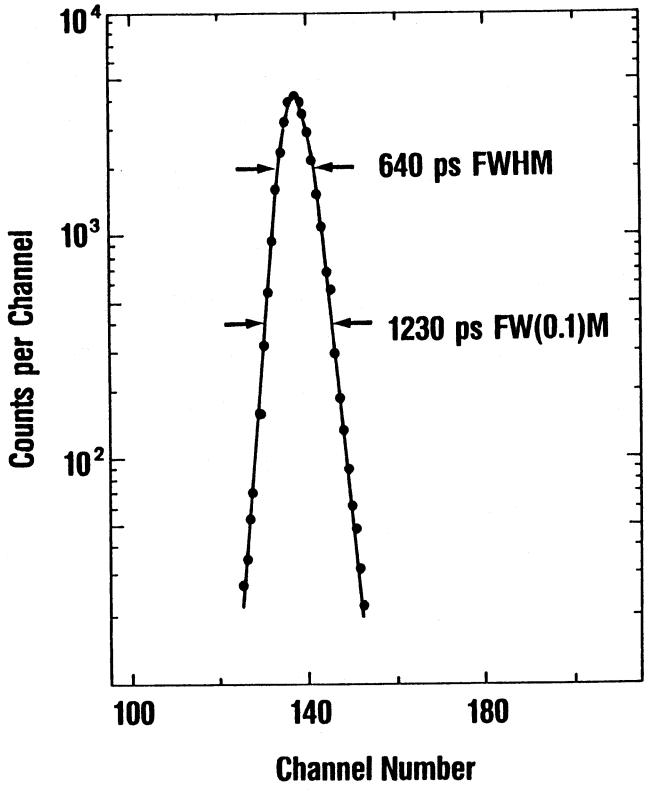

Fig. 2
Typical time resolution of a main counter element. The diagram shows the time dispersion of the coincidence peak for cosmic-ray muons traversing the 10 cm dimensions of two main counter bars. Position identification was used to eliminate events from the omnidirectional flux of muons with large zenith angles.

10 MeV and of 8% at 300 MeV for a flight path length of 4 m. The counter has already been successfully employed in recent measurements at SIN investigating the absorption of positive and negative pions [7,8].

---

[1] Now at Radiation and Radioactivity Metrology Section, Electrotechnical Laboratory, Umezono, Ibaraki, Japan

[2] Institut für Reaktorentwicklung, Kernforschungsanlage Jülich, Jülich, Fed. Rep. of Germany

[3] Guests from University of Zagreb, Zagreb, Yugoslavia

[4] Institute for Physics, University of Basel, Basel, Switzerland

References

[1] P. Cloth, D. Filges, G. Sterzenbach, T.W. Armstrong and B.L. Colborn, The KFA Version of the High-Energy Transport Code HETC and the Generalized Evaluation Code SIMPEL, Kernforschungsanlage Jülich Report, Jül-Spec-196, March 1983

[2] S. Cierjacks, Y. Hino, S.D. Howe, F. Raupp and L. Buth, Differential Neutron Production Cross Sections for 590 MeV Protons, Proc. Int. Conf. on Nuclear Data for Science and Technology, D. Reidel Publ. Comp., Dordrecht, 1983, p. 383

[3] S. Pearlstein, Summary of the Medium Energy Nuclear Data Working Group Meeting held at the Brookhaven Nat. Laboratory, to be published, 1986

[4] B.E. Bonner, J.E. Simmons, C.R. Newsom, P.J. Riley, G. Glass, C.J. Hiebert, M. Jain and L.C. Northcliffe, Phys. Rev. C18(1978)1418

[5] S. Cierjacks, New Intense Neutron Sources and Related Nuclear Data Needs, Proc. KTG/ENS Int. Sem. on Nucl. Data, Cross Section Libraries and their Application in Nucl. Technology, Bonn, 1985, p. 315

[6] S. Cierjacks, T. Petković, H. Ullrich, D. Gotta, S. Ljungfelt, N. Šimičević, M. Izycki, P. Weber and H.J. Weyer, Nucl. Instrum. Meth. in Phys. Research A238(1985)354

[7] G. Backenstoss, M. Izycki, M. Steinacher, P. Weber, H.J. Weyer, K. v.Weymarn, S. Cierjacks, S. Ljungfelt, U. Mankin, T. Petković, G. Schmidt and H. Ullrich, Phys. Lett. 137B(1984)329

[8] G. Backenstoss, M. Izycki, P. Salvisberg, P. Weber, H.J. Weyer, S. Cierjacks, S. Ljungfelt, H. Ullrich, M. Furić and T. Petković, Phys. Rev. Lett. 55 (1985)2782

KERNFORSCHUNGSZENTRUM KARLSRUHE
INSTITUT FÜR KERNPHYSIK III

1. 3.75 MV Van de Graaff-Accelerator

1.1 The ^{40}Ar Capture Cross Section and the ^{40}Ar Solar Abundance

H. Beer, R.D. Penzhorn[+]

As the natural isotopic abundance of ^{40}Ar is dominated by the radiogenic component from the ^{40}K decay the original ^{40}Ar abundance has to be estimated via the existing concepts of nucleosynthesis. Possibly, the main contribution to the nucleosynthetic ^{40}Ar abundance is due to the s-process [1,2].

In this study a detailed s-process analysis to calculate the ^{40}Ar abundance has been carried out. The synthesis of ^{40}Ar via the seed nuclei ^{40}Ca, ^{39}K, ^{36,38}Ar and ^{35}Cl is illustrated in Fig. 1. The synthesis path is characterized by complicated branchings caused by radioactive decay and (n,α) and (n,p) reactions on the species ^{41}Ca, ^{40}K, and ^{39}Ar. Among the involved cross sections the destruction of ^{40}Ar by neutron capture is of primary importance. This cross section has been measured by a special activation technique [3,4]. The ^{40}Ar sample for the irradiations was fabricated by chemical fixation of Ar in zeolite 5A [5]. The Maxwellian averaged capture cross section of ^{40}Ar at a thermal energy of kT = 23.4 keV was found to be 2.55 ± 0.15 mb.

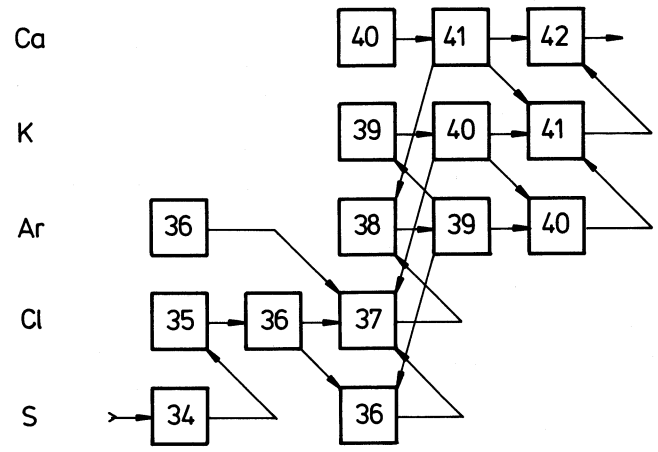

Fig. 1 The reaction network used in calculating the s-process abundance of ^{40}Ar.

The s-process calculation was carried out using the neutron exposure distribution derived from a study of s-process abundances for nuclei in the mass range A>56 [6]. For ^{40}Ar an s-process abundance 24±7 (Si≡10^6) has been obtained.

---

[1] J.G. Peters, W.A. Fowler, D.D. Clayton, Ap. J. 173 (1972) 637
[2] A.G.W. Cameron, in Essays in Nucl. Astrophysics, Cambridge University Press 1982, p. 23
[3] H. Beer, F. Käppeler, Phys. Rev. C21 (1980) 534
[4] H. Beer, F. Käppeler, G. Reffo, G. Venturini, Astrophysics and Space Sci. 97 (1983) 95
[5] R.D. Penzhorn, G. Walter, H. Beer, Z. f. Naturforschung 38a (1983) 712
[6] H. Beer, Proc. of the 5th Moriond Astrophysics Meeting, Les Arcs, Savoie 1985

+ Institut für Radiochemie, Kernforschungszentrum Karlsruhe

1.2 Neutron Capture in the 1.15 keV Resonance of ^{56}Fe Using Moxon-Rae Detectors*

F. Corvi+, C. Bastian+, K. Wisshak

The capture area in the 1.15 keV neutron resonance of ^{56}Fe was measured with Moxon-Rae detectors with converters of bismuth, bismuth-graphite and graphite. The data were normalized to Au capture at 4.91 eV using the saturated resonance method. Two separate measurements were performed, the first with the detector axis at 120° with respect to the neutron beam direction, the second with the axis at 90°. The average of the results over the three detectors is:

$g\Gamma_n\Gamma_\gamma/\Gamma$ = (64.9 ± 2.4) meV for the 120° run and
$g\Gamma_n\Gamma_\gamma/\Gamma$ = (63.5 ± 2.1) meV for the 90° run.

These values are 14 and 16 % larger than the results of a transmission measurement [1]. No reason is found for this discrepancy.

---

[1] F.G. Perey, J.H. Harvey, N.W. Hill, ORNL, priv. communication (1983)

* Nucl. Sci. Eng. (in print)

+ CEC-JRC, Central Bureau for Nuclear Measurements, B-2440 Geel, Belgium

1.3 The β^--Branch in the Decay of $^{79}Se^m$

N. Klay, F. Käppeler, G. Rupp

The β^- branch in the decay of the 96 keV isomeric state in ^{79}Se is of special importance for nuclear astrophysics because it is this transition that can greatly enhance the total beta decay rate of ^{79}Se at the high temperatures of $\sim 3 \cdot 10^8$ K prevailing during nucleosynthesis. Under such conditions, thermal equilibrium leads to a population of the excited states leaving about 1 % of the nuclei in the isomeric state. Contrary to the ground state, the isomer can decay to ^{79}Br by an allowed beta transition at a correspondingly faster rate. Log ft values of 5.4 [1] and 5.0 [2] were deduced for this decay from similar transitions in neighbouring isotopes but with uncertainties of $\sim$ 10 %.

We have measured this log ft value by determining the branching ratio between the 3.9 m ground state transition and the beta decay. Activation of an extremely clean sample - consisting of a thin carbon backing with an implanted layer of ^{78}Se - at the ILL high flux reactor in Grenoble provided the isomer $^{79}Se^m$. Besides the purity of the sample, the second problem of the experiment was the suppression of the conversion electrons from the ground state transition. This was achieved by means of a mini-orange spectrometer [3] made of samarium cobalt permanent magnets, which is shown schematically in Fig. 1. With

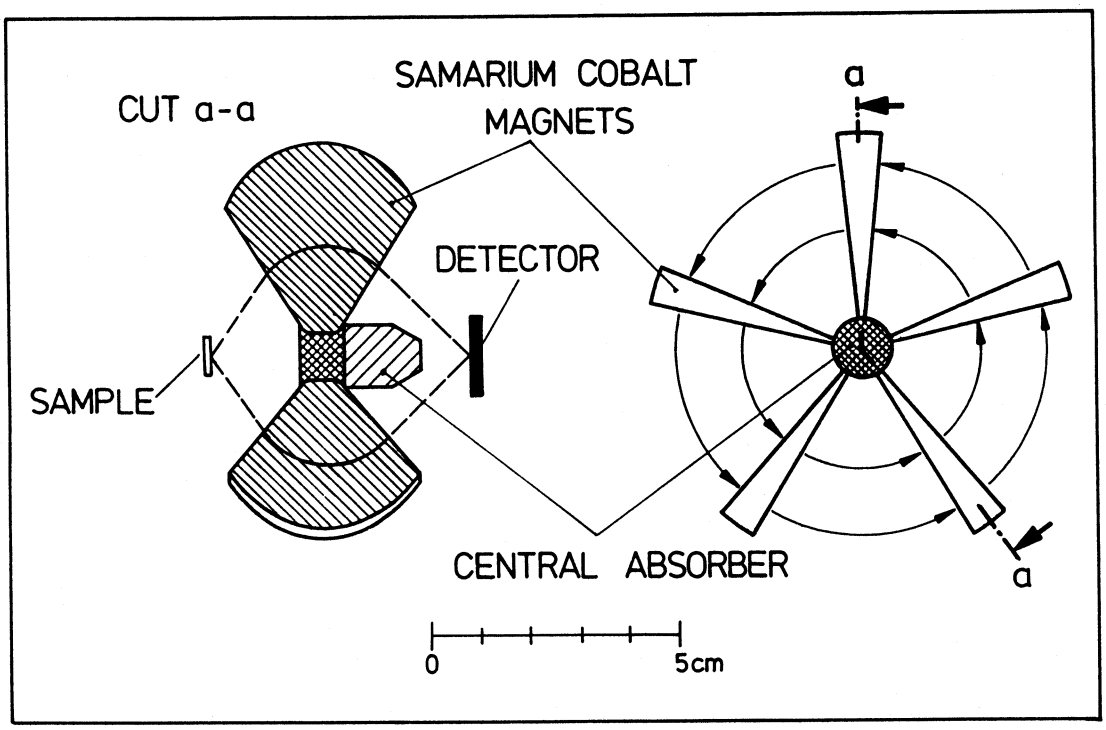

Fig. 1 Schematic setup of the mini-orange spectrometer for suppression of the conversion electron background from $^{79}Se^m \rightarrow {}^{79}Se^g$ transitions.

this spectrometer inserted between sample and detector, the conversion electrons were sufficiently suppressed to record the electrons from beta decay for about 3 half lives. Then, the mini-orange was removed and the much more intense ground state decay recorded for direct comparison. Though data analysis is not yet completed, a preliminary value of log ft = 4.6 ± 0.2 can be given for the beta transition $^{79}Se^{m} \rightarrow {}^{79}Br$.

[1] J.H. Conrad, PhD Thesis, University of Heidelberg (1976)
[2] K. Yokoi, K. Takahashi, Report KfK-3849, Kernforschungszentrum Karlsruhe 1985
[3] J. van Klinken, K. Wisshak, Nucl. Instr. Meth. 98 (1972) 1
J. van Klinken, S.J. Feenstra, G. Dumont, Nucl. Instr. Meth. 151 (1978) 433

1.4 The Isomeric Ratio of ^{85}Kr at a Thermal Energy of kT = 54 keV

F. Käppeler, A.A. Naqvi+, M. Al-Ohali+

Studies of neutron capture nucleosynthesis in the s-process usually refer to a thermal energy of kT = 30 keV, corresponding to a temperature of $T=3.5 \cdot 10^{8}$ K. This convention is justified as stellar neutron capture rates are in general not sensitive to temperature due to the approximate $E^{-1/2}$-dependence of most capture cross sections. One of the exceptions from this rule concerns the fractional population of the isomeric state in ^{85}Kr which strongly influences the s-process branching at this isotope. We have shown that activation measurements can be performed in a quasi stellar neutron spectrum for kT = 54 keV, using kinematically collimated neutrons from the $^{3}H(p,n)$ reaction. The so obtained results for $^{85}Kr^{m}$ together with earlier data measured at kT = 23 keV yield the required energy dependence for proper interpolation to kT = 30 keV.

+ University of Dhahran, Dhahran, Saudi-Arabia

1.5 Measurement of the ^{139}La Capture Cross Section and a Study of the s-Process at Magic Neutron Number 82

H. Beer

The capture cross sections of the isotopes with magic neutron number 82 at the precipice of the σN-curve are of special importance for the adjustment of the main s-process component which describes the bulk of heavy s-process elements ($90 \leq A \leq 200$). Previously, measurements on ^{138}Ba, ^{140}Ce [1] and ^{142}Nd [2] have been reported. The measurement of the ^{139}La capture cross section is a

continuation of this effort to establish reliable data for this important part of the synthesis path.

The experiment was carried out by the activation method [1] relative to the gold capture cross section. The sample characteristics and the Maxwellian averaged capture cross sections are summarized in Table I.

As the new value for ^{139}La deviates considerably from the previously adopted capture cross section ($\sigma(^{139}La) = 54 \pm 5$ mb from Musgrove et al. [3]) a new calculation of the σN-curve with the data of Table II has been carried out. For the time integrated neutron flux ($\tau_o = 0.304 \pm 0.013$ mb^{-1}) only a change of 1.5 % was found using the new ^{139}La capture cross section. Therefore, the old value of τ_o is consistent with the new result within the calculated uncertainty. The derived s-process abundance for ^{139}La of 0.33±0.03 (Si≡ 10^6) is, however, considerably larger than the previous value of 0.23±0.02 (Si≡10^6).

Table I Sample Characteristics and Maxwellian averaged Capture Cross Section of ^{139}La

Reaction	$T_{1/2}$	E_γ(keV)	I_γ(%)	$\frac{\langle\sigma v\rangle}{v_T}$ mb kT = 23.4 keV
$^{139}La(n,\gamma)^{140}La$	40.272 h	1596	95.5 ± 0.3	44.1 ± 2.9
$^{197}Au(n,\gamma)^{198}Au$	2.69 d	412	95.52± 0.06	657 ± 16

Table II Neutron Capture Cross Sections of Stable Nuclei with Magic Neutron number 82

Nucleus	$\langle\sigma v\rangle/v_T$ mb at kT = 30 keV	
^{138}Ba	3.96 ± 0.23	Ref. (1)
^{139}La	38.4 ± 2.7	this work
^{140}Ce	10.82 ± 0.53	Ref. (1)
^{141}Pr	119 ± 16	Ref. (3)
^{142}Nd	47 ± 4	Ref. (2)

Not that the capture cross sections in Refs. [1] and [2] had to be normalized due to a change in the Au standard. The most important ^{138}Ba capture

cross section is now in excellent agreement with the value $\sigma(^{138}Ba)$ = (3.8 ± 0.8) mb reported by Musgrove et al. [4].

---

[1] Beer, F. Käppeler, Phys. Rev. C21 (1980) 534
[2] G.J. Mathews, F. Käppeler, Ap. J. 286 (1984) 810
[3] A.R. de L. Musgrove, B.J. Allen, R.L. Macklin, Aust. J. Phys. 30 (1977) 599
[4] A.R. de L. Musgrove, B.J. Allen, R.L. Macklin, Aust. J. Phys. 32 (1979) 213

1.6 Measurement of the Capture Cross Sections of ^{156}Dy and $^{194m,196,198}Pt$

H. Beer

The analysis of s-process branchings is a major source of information for important astrophysical parameters like neutron and electron density and the s-process temperature [1]. As the various branchings exhibit a different sensitivity to these parameters due to the individual properties of the involved nuclei, it is desirable to analyze as many branchings as possible.

The capture cross section measurements of ^{156}Dy and of the Pt isotopes are expected to contribute to a better analysis of the ^{157}Gd and ^{192}Ir branchings. The measurements were carried out with the activation technique. The experimental arrangement is a standard setup at the Karlsruhe Van de Graaff accelerator and has been described in detail elsewhere [2,3]. The decay properties, the induced activities, and the Maxwellian averaged capture cross sections are summarized in Table I.

In branching analyses, the rates for beta decay and neutron capture of the branch point isotope, but also the capture cross section of a stable s-process isotope on one of the branches are of primary importance. This signifies for the ^{157}Gd and ^{192}Ir branchings that improved capture cross sections of ^{158}Dy and ^{192}Pt, respectively, are needed. The measured capture cross sections on ^{156}Dy, $^{194m,196,198}Pb$ are useful to derive better statistical model parameters for the individual nuclei in the isotopic chain, especially for ^{158}Dy and ^{192}Pt.

Table I Decay Properties and measured Capture Cross Sections (preliminary)

Reaction	$T_{1/2}$	E_γ(keV)	I_γ(%)	$\frac{\langle\sigma v\rangle}{v_T}$ (mb) kT = 23.4 keV
$^{156}Dy(n,\gamma)^{157}Dy$	8.1 h	326	94 ± 2	1741
$^{194}Pt(n,\gamma)^{195}Pt^m$	4.02 d	99	11.1 ± 1.1	31
$^{196}Pt(n,\gamma)^{197}Pt^m$	94.4 min	346	11.1 ± 0.5	13.2
$^{196}Pt(n,\gamma)^{197}Pt$	18.3 h	77	17 ± 1	213
$^{198}Pt(n,\gamma)^{199}Pt$	30.8 min	543	15	75.6
$^{197}Au(n,\gamma)^{198}Au$	2.69 d	412	95.5 ± 0.06	657

[1] H. Beer, G. Walter, R.L. Macklin, P.J. Patchett, Phys. Rev. C30 (1984) 464
[2] H. Beer, F. Käppeler, Phys. Rev. C21 (1980) 534
[3] H. Beer, F. Käppeler, G. Reffo, G. Venturini, Astrophys. and Space Sci. 97 (1983) 95

1.7 Fission Fragment Properties in Fast-Neutron-Induced Fission of ^{237}Np*

A.A. Naqvi+, F. Käppeler, F. Dickmann, R. Müller++

We have performed a complete (2E,2v) experiment of the kinetic energies E and velocities v of correlated fragments from fast-neutron-induced fission of ^{237}Np. The influence of excitation energy on the important fragment properties as mass, kinetic energy and prompt neutron emission have been investigated experimentally at 0.80 and 5.55 MeV neutron energy. Our results include mean values of fragment properties before and after neutron evaporation, e.g., of fragment velocities and masses, total kinetic energies, and the respective variances. Also given are the distributions of fragment mass, of $E_{k,tot}$, the variance of $E_{k,tot}$ as well as the number of prompt fission neutrons as a function of fragment mass. These results show that shell effects are strong near threshold at E_n = 0.80 MeV, but decrease significantly at the higher excitation energy, in qualitative agreement with the model of Wilkins, Chasman and Steinberg [1]. However, the observed increase in the number of prompt fission neutrons, which appears only in the heavy fragment, cannot be explained by this model.

---

[1] B.D. Wilkins, E.P. Steinberg, R.R. Chasman, Phys. Rev. C14 (1976) 1832

* Phys. Rev. C (in print)

+ University of Dhahran, Dhahran, Saudi-Arabia
++ Now at Siemens AG, D-8000 München, Fed. Rep. of Germany

KERNFORSCHUNGSZENTRUM KARLSRUHE
INSTITUT FÜR NEUTRONENPHYSIK UND REAKTORTECHNIK

1. Nuclear Reaction Theory

1.1 Monte Carlo Sampling from the Statistical-Model Distribution of R-Matrix Elements

F.H. Fröhner

The joint maximum-energy distribution of the R-matrix elements R_{ab} has been found to be a generalised Student distribution,

$$p(R|\bar{R})d\mu(R) = C \frac{\prod_{a\le b} dX_{ab}}{\det(1+X^2)^{(n+1)/2}} ,$$

$$C = \pi^{-n(n+1)/4} \frac{\Gamma((n+1)/2)}{\Gamma(1/2)} \prod_{c=1}^{n} \frac{\Gamma(n-c+1)}{\Gamma((n-c)/2+1)} ,$$

$$-\infty < X_{ab} \equiv \frac{R_{ab} - R^{\infty}_{a}\delta_{ab}}{\pi\sqrt{s_a s_b}} < \infty , \qquad (1)$$

given the usual constraints of the level-statistical model of compound-nuclear reactions, viz. unitary and symmetric S-matrix with causal analytic structure (no poles in the upper half of the complex energy plane), see [1, 2]. (The corresponding distribution of S-matrix elements, the multi-dimensional Poisson kernel [1, 2], was independently found by Mello, Pereyra and Seligman [3]). This result offers the possibility for simplified sampling of reaction cross sections, for instance in the context of self-shielding and multiple-scattering corrections to neutron scattering or capture data in the unresolved resonance region [4]. The conventional method is sampling of resonance parameters (energies from the GOE distribution, partial widths from the appropriate Porter-Thomas distributions) for a statistically adequate number of levels. From these one can calculate the R-matrix elements and finally the cross sections of interest. With the distribution (1) it is possible to sample the R-matrix elements directly without invoking a large number of resonances and their parameters.

A method for rapid sampling from (1) is being tested. It is based on the recursion relations for integrals of the type

$$I_n(\alpha) = \int \frac{d\mu(X)}{\det(1+X^2)^{\alpha}}$$

given by Hua [5].

References

[1] F.H. Fröhner, Proc. Int. Conf. on Nuclear Data for Basic and Applied Science, Santa Fe, New Mexico, May 13-17, 1985 (in print)

[2] F.H. Fröhner, Proc. Spec. Meet. on Use of the Optical Model for the Calculation of Neutron Cross Sections Below 20 MeV, Paris, 13-15 Nov. 1985, NEANDC-222 'U' (1986)

[3] P.A. Mello, P. Pereyra, T.H. Seligman, Ann. Phys. 161 (1985) 254. The significance of the Poisson kernel seems first recognised in T.H. Seligman, Escuela Latinoamericana de Fisica, Cali, Colombia 1982 (World Scient. Publ., Singapore) p. 674; see also P. Mello, Conf. on Nucl. Reaction Mechanisms, Varenna, 1982, p. 69

[4] F.H. Fröhner, "Applied Neutron Resonance Theory", in Nuclear Theory for Applications, IAEA Vienna (1980); available also as KfK 2669 (1978)

[5] L.K. Hua, Harmonic Analysis of Functions of Several Complex Variables in the Classical Domains (American Math. Soc., Providence, Rhode Island, 1963)

INSTITUT FÜR CHEMIE (1): NUKLEARCHEMIE
KERNFORSCHUNGSANLAGE JÜLICH

1. Neutron Data

1.1 Fundamental Studies on Complex Particle Emission Reactions

S.M. Qaim, R. Wölfle

In continuation of our radiochemical studies on fast neutron induced tri-nucleon emission reactions we measured in collaboration with CBNM Geel (H. Liskien) the excitation functions of $^{181}Ta(n,t)^{179}Hf$ and $^{93}Nb(n,^{3}He)^{91}Y$ reactions over the neutron energy range of 16 to 19 MeV. As expected the cross sections were low (μb region). The energy dependence of an $(n,^{3}He)$ reaction has been investigated for the first time and the results are shown in Fig. 1. Detailed Hauser-Feshbach calculations on the first-chance emission of an ^{3}He-particle showed that the contributions of statistical processes are small [1]. The ratio of ^{3}He- to ^{3}H-emission cross section in the interaction of fast neutrons with niobium was found to increase rapidly above 17.5 MeV. However, the fact that even at high excitation energy (e.g. with 53 MeV d(Be) break-up neutrons) the ratio is <1 suggests that ^{3}He-emission is intrinsically a weaker phenomenon than ^{3}H-emission.

The energy dependence of the $^{58}Ni(n,d)^{57}Co$ reaction was also determined for the first time [2], and the results are given in Fig. 2. The cross section increases rapidly beyond 8 MeV, reaching almost the maximum value at about 15 MeV. Hauser-Feshbach calculations show that beyond 11 MeV the relative contribution of the statistical processes decreases and at about 15 MeV it is <30 % of the total (n,d) cross section. Calculations involving precompound effects seem to agree with the experimental trend over the energy range of 9 to 15 MeV within a factor of 2.

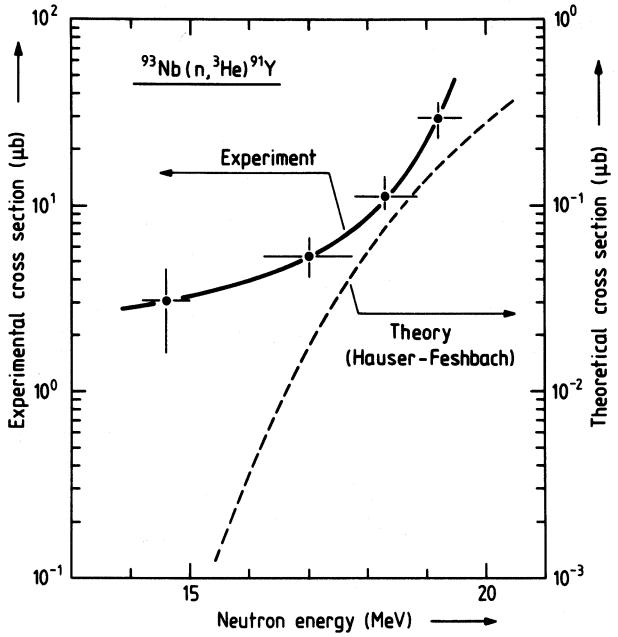

Fig. 1 Excitation function of the $^{93}Nb(n,^{3}He)^{91}Y$ reaction [1].

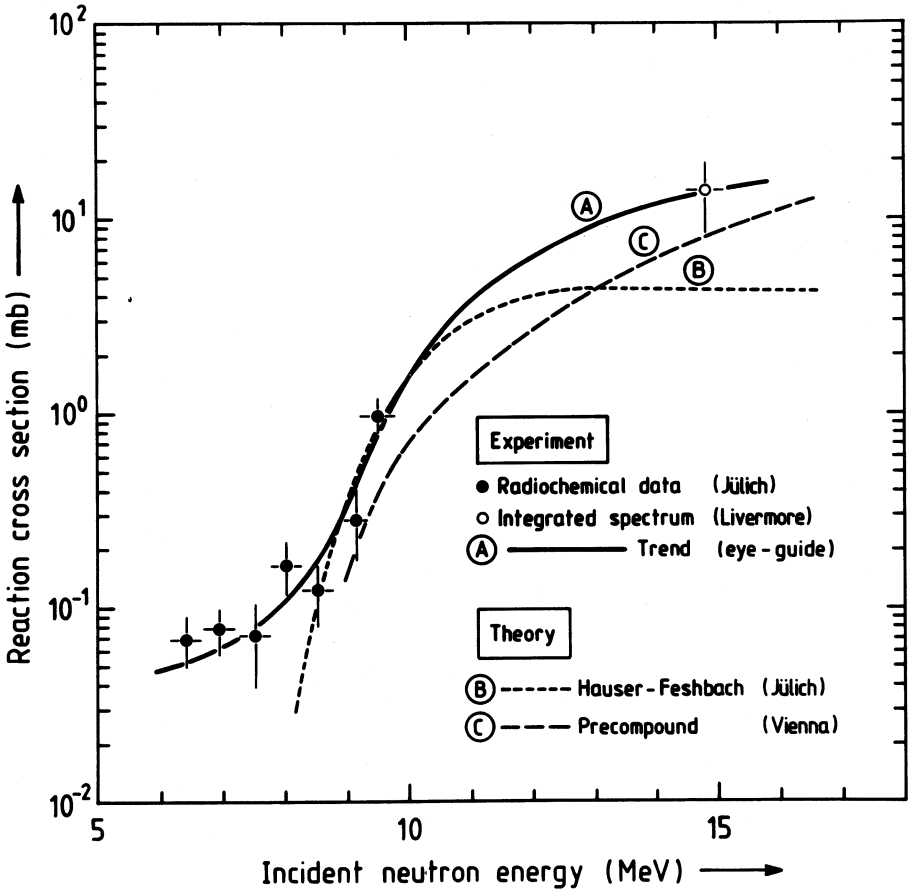

Fig. 2 Excitation function of the $^{58}Ni(n,d)^{57}Co$ reaction [2].

1.2 Cross Section Data Relevant to Fusion Reactor Technology

R. Wölfle, A. Suhaimi, S.M. Qaim

(Relevant to request identification numbers: 724008F, 762246F, 781211F, 801238F, 832045F)

Triton emission cross sections in the interactions of fast neutrons with light nuclei ^{7}Li, ^{10}B and ^{9}Be were determined. Measurements on the $^{7}Li(n,n't)^{4}He$ reaction were performed in the incident neutron energy range of 8 to 10.5 MeV. The data fit well in the trend reported earlier. Cross section measurements on the $^{10}B(n,t)2\alpha$ reaction reported last year [3] were extended up to 10.5 MeV. In addition to B_4C samples enriched ^{10}B samples were also used. The results were found to be consistent. Investigations on the $^{9}Be(n,t)2\alpha$ reaction in the energy range of 13 to 20 MeV have been initiated in collaboration with CBNM Geel (H. Liskien).

Cross sections for the $(n,n\alpha)$ reactions on ^{51}V, ^{92}Mo, ^{115}In, ^{165}Ho and ^{176}Yb were measured radiochemically at $E_n = 14.7 \pm 0.3$ MeV. A tentative trend in the data is shown in Fig. 3 [4]. The contribution of the $(n,n\alpha)$ process generally amounts to between 10 and 15 % of the (n,α) cross section; in some cases, however, it is as low as 0.5 %. This

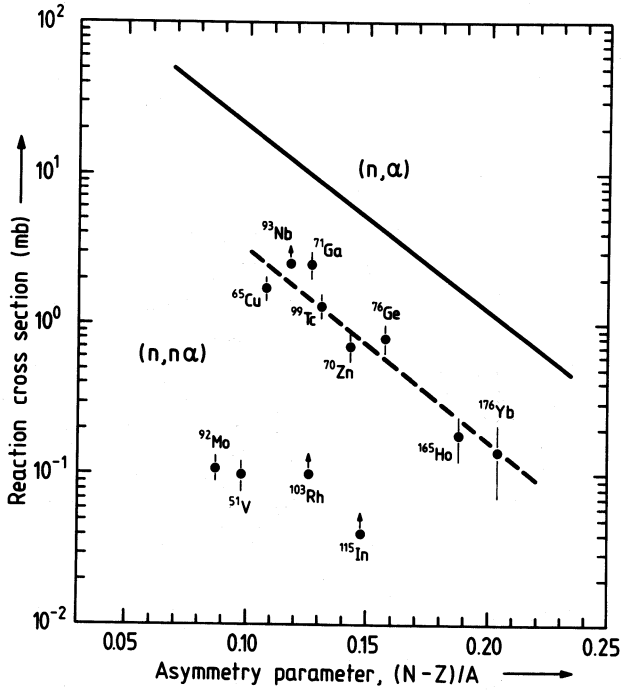

Fig. 3 Systematics of activation cross sections of $(n,n\alpha)$ reactions induced by 14.7 ± 0.3 MeV neutrons. The solid line describes the gross trend in (n,α) reaction cross sections and has been drawn for comparison.

observation leads to the conclusion that the role of the (n,nα) process in total helium emission is not as important as of (n,np) process in total hydrogen emission.

2. Charged Particle Data for Radioisotope Production

S.M. Qaim, G. Stöcklin

In continuation of our studies [cf. 5] on the production of medically important short-lived β^+-emitting radioisotopes excitation functions of (α,xn) reactions on ^{75}As, relevant to the formation of ^{78}Br ($T_{1/2}$ = 6.5 min) and ^{77m}Br ($T_{1/2}$ = 4.3 min), were measured [6]. The data are reproduced in Fig. 4. They appear to agree with the systematics of cross sections in this mass region. The

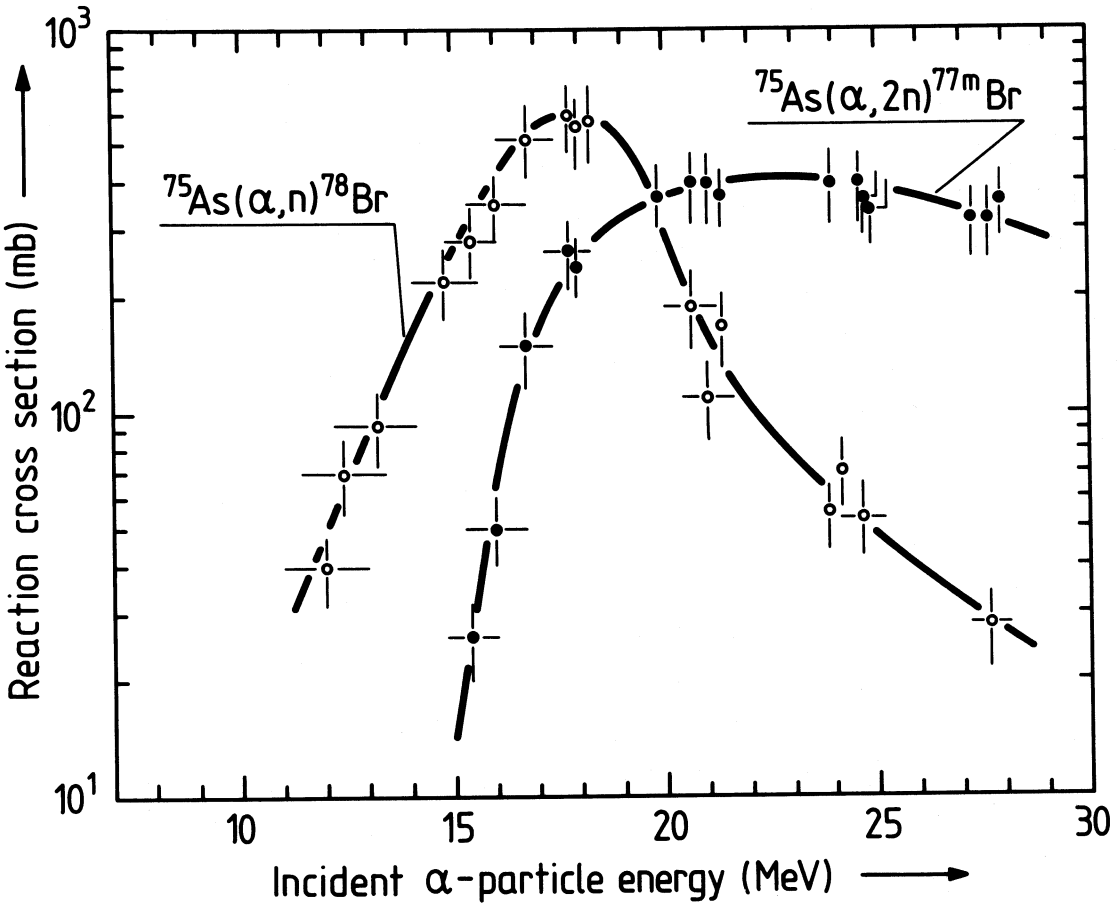

Fig. 4 Excitation functions of the (α,xn) reactions on ^{75}As [6].

thick target saturation yield of the β^+-emitter ^{78}Br over the energy range of E_α = 28 → 10 MeV amounts to 13 mCi/μA. A 30 min irradiation with 28 MeV α-particles at 25 μA could thus lead to (theoretically) about 325 mCi ^{78}Br.

Some cross section measurements on the formation of ^{75}Br ($T_{1/2}$ = 1.6 h) via the ^{74}Se(d,n)^{75}Br reaction were carried out and the possibility of using this reaction at a low energy cyclotron was investigated. Furthermore, measurements of cross sections of α-particle induced reactions on Ge, relevant to the production of ^{73}Se ($T_{1/2}$ = 7.1 h), a potentially useful β^+-emitter, were initiated.

References

[1] S.M. Qaim, R. Wölfle, H. Liskien, Excitation function of ^{93}Nb(n,^{3}He)^{91}Y reaction near its threshold: Comparison of ^{3}He- and ^{3}H-emission probabilities, Phys.Rev.C, in press

[2] S.M. Qaim, R. Wölfle, Excitation function of the ^{58}Ni(n,d)^{57}Co reaction near its threshold, Phys.Rev. C 32 (1985) 305

[3] S.M. Qaim, R. Wölfle, G. Stöcklin, M. Rahman, S. Sudar, A. Suhaimi, Determination of (n, charged particle) reaction cross sections for FRT-relevant materials, Proc. Int. Conf. on Nuclear Data for Basic and Applied Science, Santa Fe, New Mexico, USA, 13 to 17 May 1985, in press

[4] S.M. Qaim, A study of (n,nα) reaction cross sections at 14.7 MeV, Nucl.Phys.A, in press

[5] Z. Kovács, G. Blessing, S.M. Qaim, G. Stöcklin, Production of ^{75}Br via the ^{76}Se(p,2n)^{75}Br reaction at a compact cyclotron, Int.J.Appl. Radiat.Isotopes 36 (1985) 635

[6] S.M. Qaim, G. Blessing. H. Ollig, Excitation functions of ^{75}As(α,n)^{78}Br and ^{75}As(α,2n)^{77m,g}Br reactions from threshold to 28 MeV, Radiochimica Acta, in press

INSTITUT FÜR REINE UND ANGEWANDTE KERNPHYSIK
UNIVERSITÄT KIEL, GKSS-FORSCHUNGSZENTRUM GEESTHACHT

Fast-Chopper Neutron Time-of-Flight Spectrometer

H.G.Priesmeyer

After completion of a transmission measurement on radioactive I-129 (86.1 At% enrichment) on July 11, 1985 the Kiel university fast chopper time-of-flight spectrometer has been shut down, dismantled and preserved. Therefore within reasonable space of time this unique instrument for the investigation of highly radioactive sample material will be no more available.
The analysis of the I-129 resonances is in progress (relevant to WRENDA 812037N).
The transmission spectrum of an optimized iron filter and an iron-titanium difference filter both have been fitted by analytic expressions, which allow to calculate improved values for the average and variance of energy dependent cross sections. The total hydrogen cross section has been determined by this procedure to be

$$17.70 \pm 0.04 \text{ barn} \quad \text{at} \quad 23.965 \pm 0.835 \text{ keV}$$

This result is in very good agreement with theory, using the parameters of LOMON and WILSON for the effective range model.
One may conclude that the iron-titanium filter difference method can be successfully used for the determination of cross section standards.
The Sc filter of the PTB Braunschweig has been investigated in the 2 keV range. A Cu contamination of the Sc of 2 At% has been deduced from the transmission analysis of the 2.038 keV resonance in Cu-63 .
A 400 keV liquid neon neutron filter has been designed and awaits funding for construction.

Publications

H.G.Priesmeyer, P.Fischer, U.Harz, P. Henkens
Der totale Neutronenwirkungsquerschnitt des Wasserstoffs bei 24 keV.
Verhandlungen DPG 3 (1985) 381

H.G.Priesmeyer, P.Fischer, U.Harz, P.Henkens
The total n,p cross section at the iron-titanium filter difference energy
Nuclear Data for Basic and Applied Science, Santa Fe, May 1985, Conference Proceedings

H.G.Priesmeyer, A. Brusegan, M. Matzke
Investigations on an optimized 24 keV neutron beam filter,
to be published

H.G.Priesmeyer, P.Fischer, U.Harz
The resonance parameters of the lowest neutron level in Dy-162
ATKE 48 (1986) 55

B.Asmussen
Transmission und Auflösung eines Chopper-Systems für epithermische Neutronen
GKSS 85/E/49

B.Asmussen, H.G.Priesmeyer
The Kiel university fast-chopper neutron time-of-flight spectrometer: MONTE CARLO model and experimental test,
accepted for publication in Nucl.Instr.Meth.

H.G.Priesmeyer, U.Harz
Neutronen-Resonanzniveaus des radioaktiven J-129 unterhalb 2 keV
DPG Verhandlungen 4 (1986) 633

I. INSTITUT FÜR EXPERIMENTALPHYSIK
UNIVERSITÄT HAMBURG

1. Neutron Emission in (p,n) Reactions on Cu and Mo Isotopes

Y. Holler, R. Langkau, E. Mordhorst, W. Scobel, M. Trabandt

The neutron time-of-flight spectrometer [1] at the Hamburg Isochronous Cyclotron allows to measure continuous spectra for $3^{o} \leq \Theta \leq 177^{o}$ down to the 10-100 μb/sr·MeV level. We have studied with 26 MeV projectile the influence of residual interactions in the typical preequilibrium (PE) region of the energy spectra, and the PE nucleon emission into the backward hemisphere. The results can be summarized as follows:

(1) The angle integrated energy spectra show structures for residual excitation energies $U \leq 6$ MeV that can be traced back [2] to the $1p(1n)^{-1}$ partial state densities and are pronounced at neutron or proton shell closures.

(2) With N or Z being 3 or more units away from these shell closures the spectra become smoother, because the single particle states deviate less from an equidistant spacing. Pairing is now the dominant residual interaction resulting in characteristic odd-even effects [3] and should be taken care of in calculation with semiclassical nucleon-nucleon scattering models such as the geometry dependent hybrid model (GDH), see Fig. 1.

(3) PE emission of neutrons in the backward hemisphere considerably exceeds the predictions of all semiclassical models presently in discussion, whereas the model of Feshbach et al. [4] succeeds in reproducing them without parameter adjustment. For practical purposes the parameterization of Kalbach and Mann [5] does a reasonable job, although it underestimates the very forward yield [Fig. 2a].

The data obtained for ^{65}Cu and $^{92-100}$Mo are available on request.

2. Inclusive Neutrons from (He,xn) Reactions

F. Binasch, A. Kaminsky, H. Krause, R. Langkau, W. Scobel

Neutrons from ^{3}He induced reactions on ^{12}C, ^{27}Al, ^{63}Cu, ^{93}Nb and ^{197}Au have been measured with the apparatus [1] and projectile energies of 26.0, 34.4 and 43.1 MeV. For all targets and projectile energies the majority of neutrons is of the evaporate or multistep compound emission type, as indicated by almost isotropic angular distribution (Fig. 3). Medium and high energy neutrons originate from PE processes and inelastic as well as elastic projectile break up. An analysis of the data in the framework of a break up model [7] is in progress with emphasis on a consistent description of break up neutrons, protons and deuterons.
For energies beyond the threshold of the elastic break up (Q = -7.7 MeV), the neutron angular distributions can be compared with pure PE model calculations or parameterizations; Fig. 2b shows that the predictive power of [5] in contrast to the (p,xn) case (Fig. 2a) is only moderate, in particular at very forward angles. This observation emphasizes that PE emission is an entrance channel effect such that angular distributions cannot be adequately described only in terms of the ejectile energy.

3. Proton Induced Fission of $^{235,236,238}U$

M. Strecker, R. Wien, W. Scobel

Neutrons measured in coincidence with fission fragments under correlation angles $\Theta = 0^{o}$ and 90^{o} with respect to the fragment direction may be separated into pre- and postfission component by means of an iterative procedure assuming isotropic emission in the rest frame of the emitting nucleus. We have improved our set up [8] in two respects: The neutron TOF paths have been equipped with 10"ϕ × 2" NE213 scintillators, and the fragments are now measured with two pairs of large ($A \approx 800$ mm^2) surface barrier detectors allowing pulse height and TOF spectroscopy of the fragments [9]. The fragment mass resolution obtained is $\Delta m \approx 3$ u, the total kinetic energies are measured with an accuracy $\Delta E_{Fiss} \approx 2$ MeV (fwhm).
Measurements have been performed for E_p = 12.7, 15.2, 20.2 and 25.7 MeV. The pre- and postfission neutron multiplicities obtained follow the systematics reported earlier; in particular they confirm the increase of the prefission neutron multiplicity with increasing projectile energy (Fig. 5).

For pulse height spectroscopy of the fragments the Schmitt calibration was applied with recent calibration parameters [9]. The resulting total kinetic energies are listed in Table I, the provisional masses m_p are shown in Fig. 4. The time-of-flight measurement allows an independent determination of the fragment masses m* prior to neutron emission; the comparison in Fig. 4 reveals, that m_p and m* differ by more than the correction that are usually applied to m_p to take care of the multiplicity of emitted neutrons.

References

[1] Y. Holler, A. Kaminsky, B. Scharlemann, H. Krause, R. Langkau, W. Peters, G. Poppe, N. Schirm, W. Scobel and R. Wien, Nucl. Instr. Meth. A235 (1985)123

[2] W. Scobel, M. Blann, T.T. Komoto, M. Trabandt, S.M. Grimes, L.F. Hansen, C. Wong and B.A. Pohl, Phys. Rev. C30(1984)1480

[3] E. Mordhorst, M. Trabandt, A. Kaminsky, H. Krause, W. Scobel, R. Bonetti and F. Crespi, Phys. Rev. C (1986), in press

[4] H. Feshbach, A. Kerman and S. Koonin, Ann. Phys. (N.Y.) 125(1980)429

[5] C. Kalbach and F.M. Mann, Phys. Rev. C23(1981)112

[6] M. Blann, L.F. Hansen, T.T. Komoto, B.A. Pohl, C. Wong, S.M. Grimes, Y. Holler, W. Scobel and M. Trabandt, Proc. Workshop COPECOS (Bad Honnef, 1984), p. 46

[7] J. Kleinfeller, J. Bisplinghoff, J. Ernst, T. Mayer-Kuckuk, G. Baur, B. Hoffmann, R. Skyam, F. Rösel and D. Trautmann, Nucl. Phys. A370(1981)205

[8] P. Plischke, R. Langkau, W. Scobel and R. Wien, Nukleonika 27(1982)285

[9] K. Paasch, H. Krause and W. Scobel, Nucl. Instr. Meth. 221(1984)558

Table I: Total Kinetic Energies of $p+^{235,236,238}U$ Fragments after Neutron Emission (all Energies in MeV)

E_p	Isotope		
	^{235}U	^{236}U	^{238}U
15.2	168.4	167.8	168.8
20.2	167.1	165.0	167.4
25.7	166.6	166.0	167.3

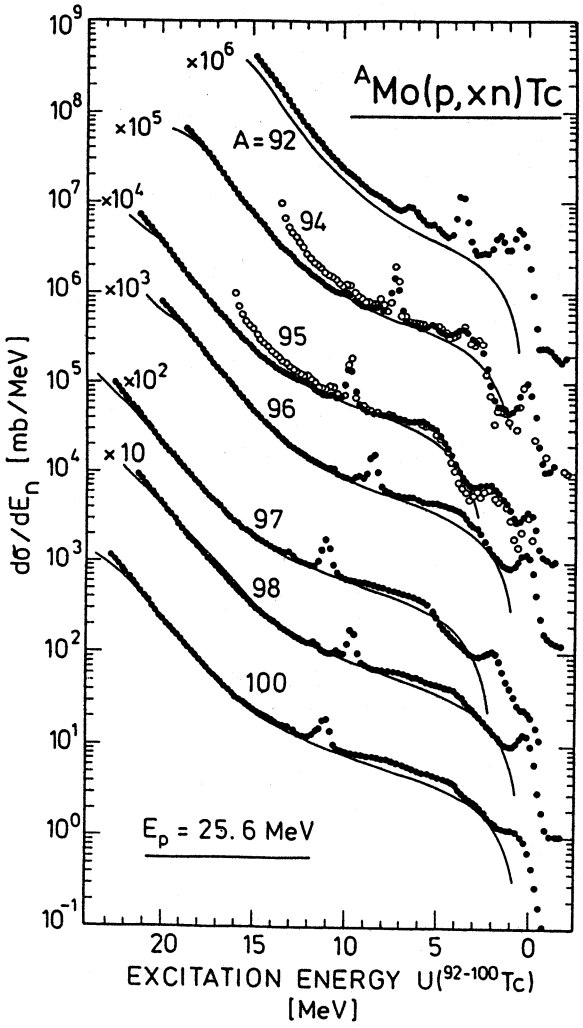

Fig. 1 Angle integrated neutron energy spectra (solid dots: this work; open circles: Ref. [6]). The solid lines denote the GDH plus evaporation model calculations including pairing corrections.

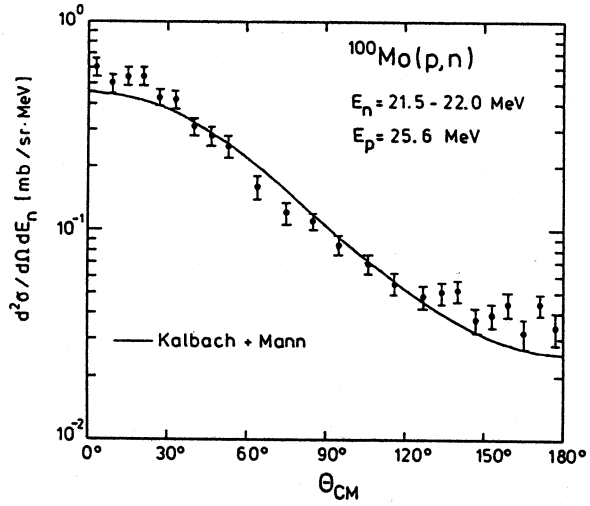

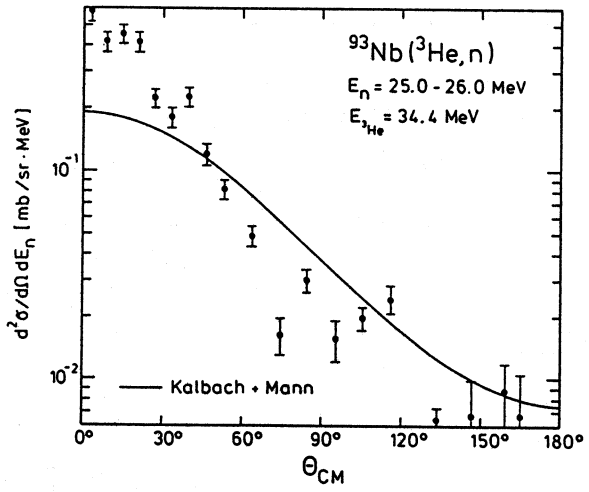

Fig. 2 Angular distributions of inclusive neutron measurements in comparison with the predictions of [5] for (a) ^{100}Mo(p,xn) with E_p = 25.6 MeV and (b) ^{93}Nb(^{3}He,xn) for $E_{^3He}$ = 34.4 MeV.

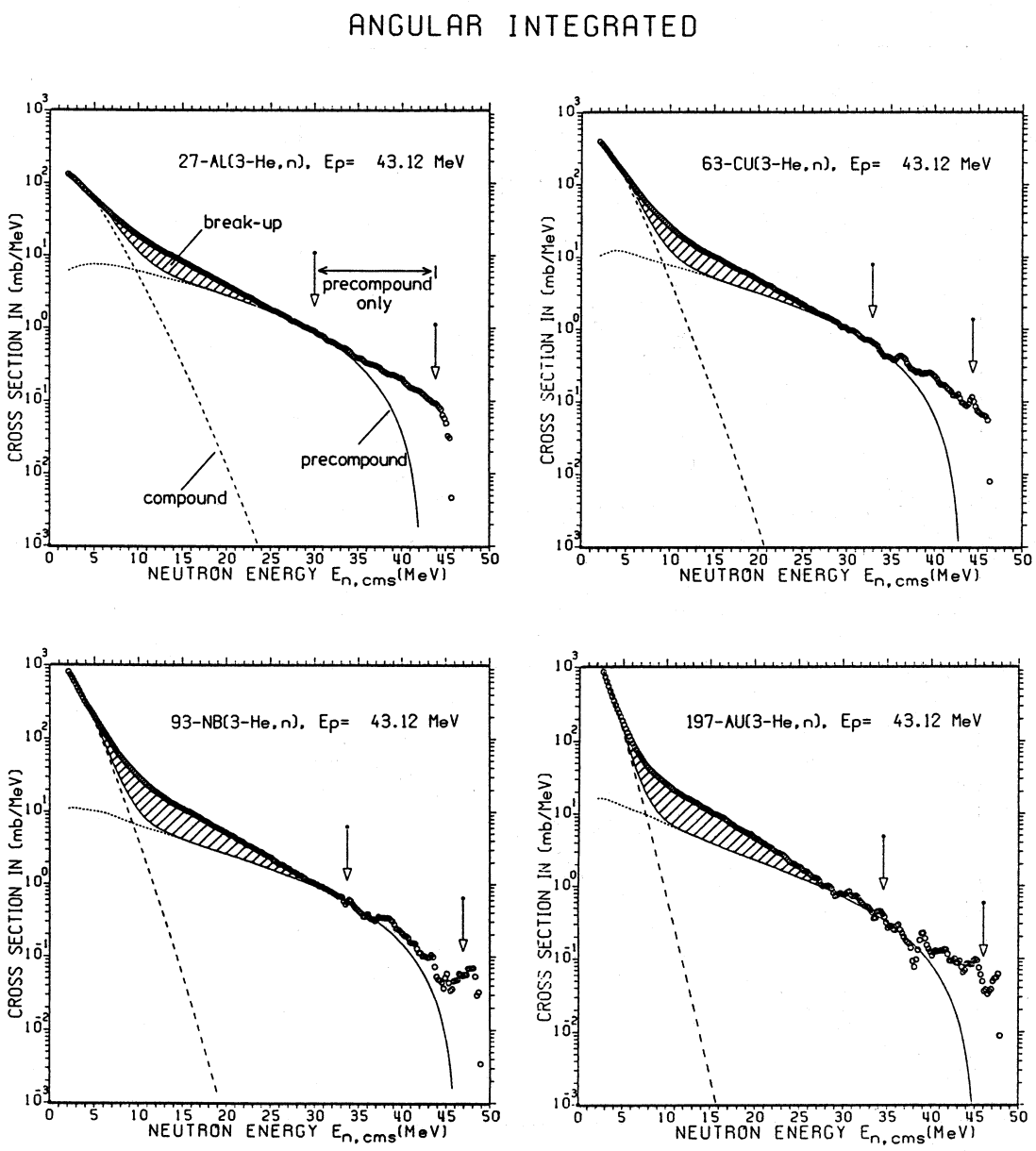

Fig. 3 Angle integrated neutron energy spectra from (^{3}He,xn) reactions of 43.12 MeV projectiles on ^{27}Al, ^{63}Cu, ^{93}Nb, ^{197}Au. Calculations: Sum (solid line) of Ewing-Weisskopf (dashed) and phenomenological [5] precompound (dotted). The arrows indicate the g.s. and break up threshold, respectively.

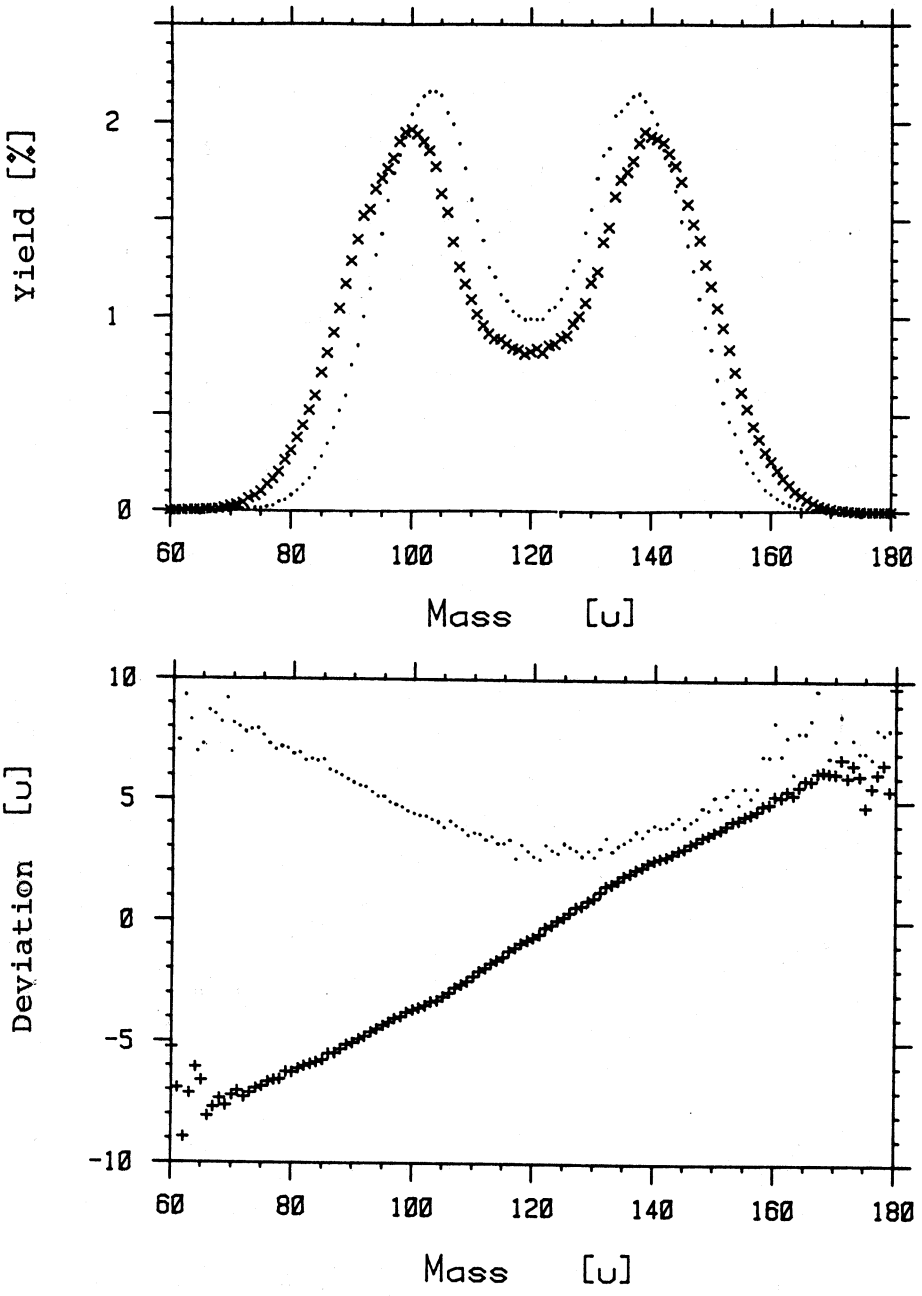

Fig. 4 Top: Distribution of fragment masses m_p (dots) and m* (crosses) from p+^{238}U for E_p = 20.2 MeV. Bottom: Difference m^*-m_p (crosses) and r.m.s. deviation $\langle(m^*-m_p)^2\rangle^{1/2}$.

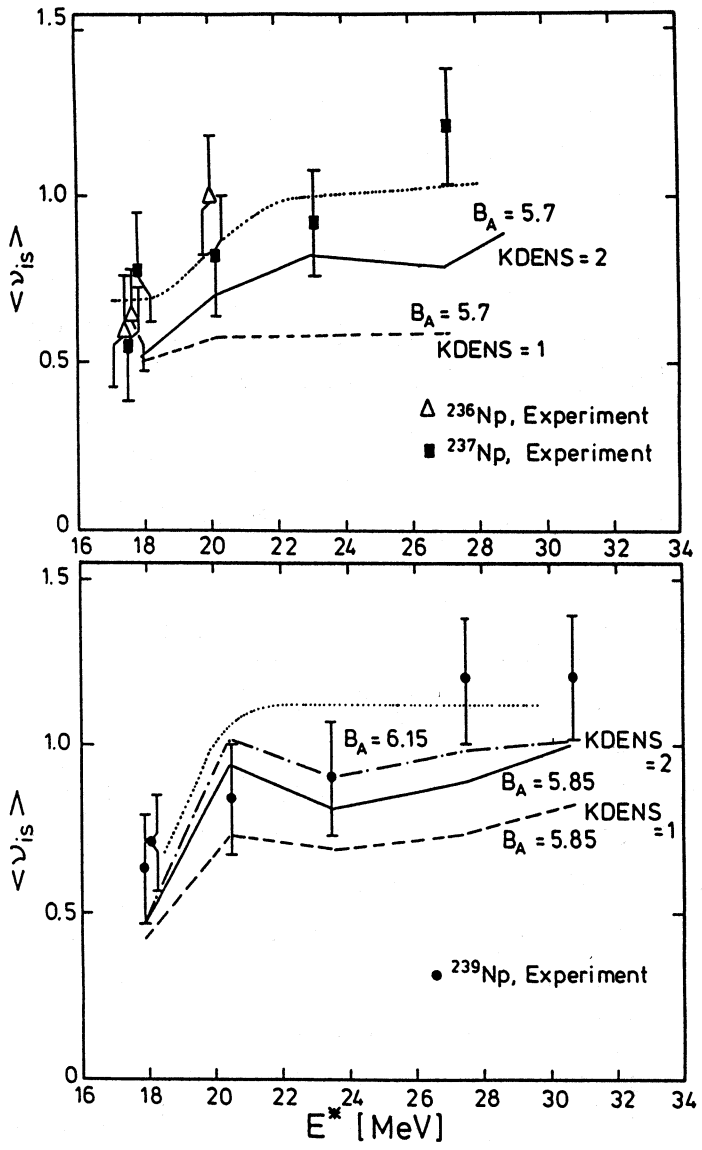

Fig. 5 Multiplicity $\langle \nu_{iso} \rangle$ of prefission plus scission neutrons vs. excitation energy E* of the initial compound system ^{236,237,239}Np. The experimental data are compared with statistical model calculations for a height B_A of the first barrier (in MeV) and a triaxial (KDENS = 1) or axialsymmetric (KDENS = 2) saddle point shape.

INSTITUT FÜR BIOCHEMIE
ABTEILUNG NUKLEARCHEMIE
UNIVERSITÄT ZU KÖLN

1. Thin Target Cross Sections and Thick Target Production Rates for the Interpretation of Cosmogenic Nuclides in Extraterrestrial Matter

P.Dragovitsch, F.Peiffer, S.Theis, R.Michel[+]

1.1 Experimental and Theoretical Production Rates of Spallogenic Nuclides in Artificial Meteorites

In a series of 600 MeV irradiation experiments at the CERN-SC the interaction of galactic protons with small meteorites was simulated. Three artificial meteorites with radii of 5, 15 and 25 cm made of diorite and gabbro were used as targets. The latter materials are particulary suitable to simulate stony meteorites because their high density, low water contents and chemical composition. The artificial meteorites contained at various locations a variety of pure element foils, selected chemical compounds and degassed meteoritic material. The cosmic 4π isotropic irradiation was simulated by the artificial meteorites performing complex movements during irradiation. Fig.1 shows the arrangement used to irradiate the R=15 and 25cm artificial meteorites and indicates the data of the target movements in the R=25cm case.
Depth profiles for the production of spallogenic radionuclides as well as of stable rare gas isotopes were measured using gamma-spectrometry, conventional and accelerator mass spectrometry. More than 400 depth profiles have been measured so far. Results for the R=5cm artificial meteorite and some preliminary data for the second and third one have already been published [1,2 and references therein, 3-6]. Fig.2 shows the depth profi-

[+] Now at Zentraleinrichtung für Strahlenschutz, Univ. Hannover

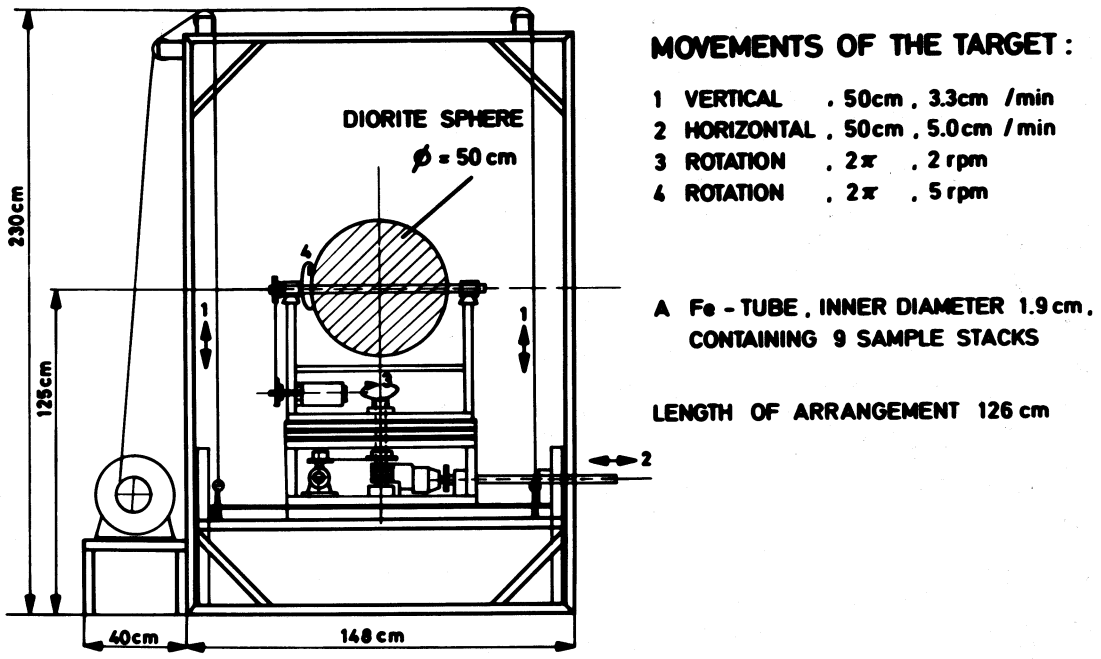

Fig. 1 Target arrangement used in the second and third irradiation of experiment CERN SC96.

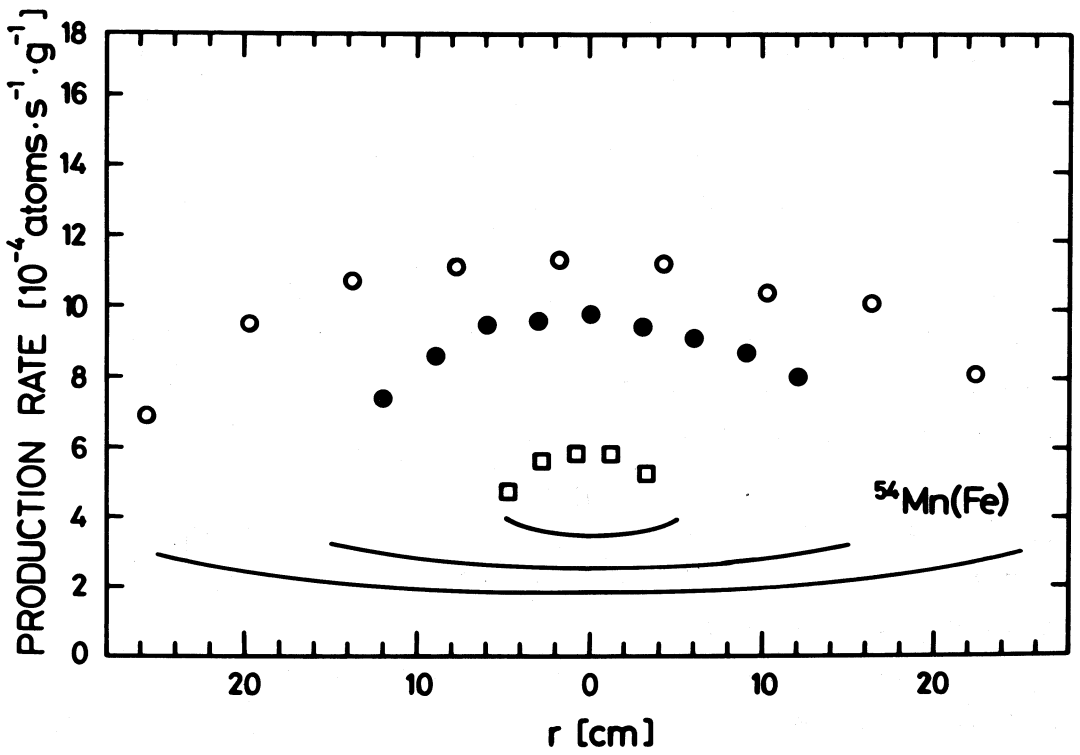

Fig. 2 Production of ^{54}Mn from Fe in artificial meteorites with radii of 5, 15 and 25cm (o, ●, □ experimental results). The full lines give the calculated production due to primary protons only.

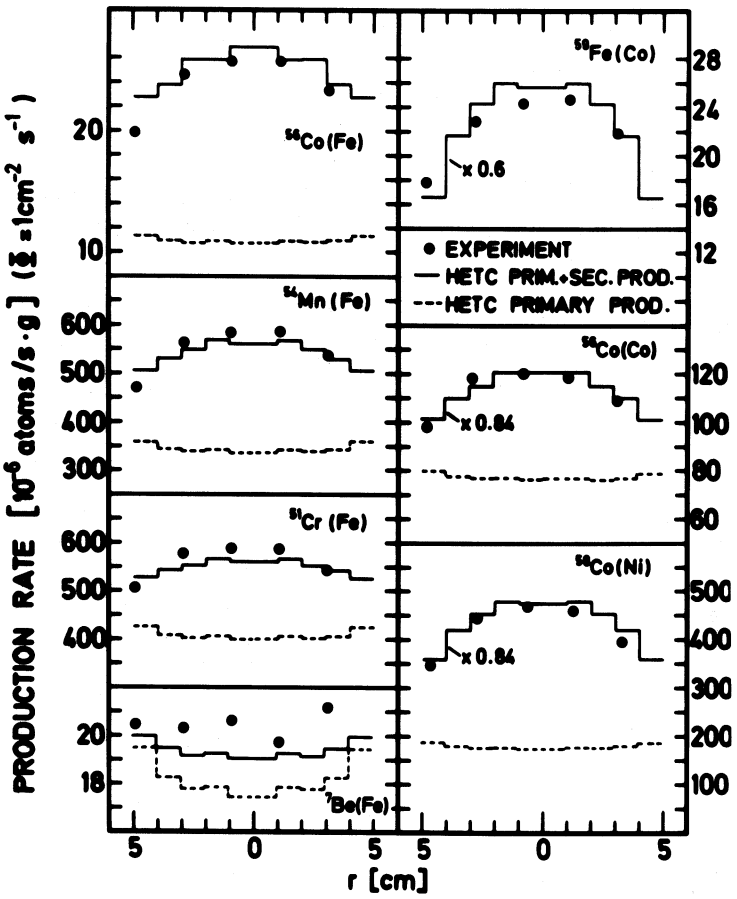

Fig.3 Comparison of experimental depth profiles of some selected radionuclides in the R=5cm artificial meteorite with results of Monte Carlo calculations.

les for the production of ^{54}Mn from Fe obtained in three artificial meteorites. A comparison of the experimental data with the production rates due to primary protons only (full lines) strikingly demonstrates the importance of secondary reactions also in small meteorites. The large number of data obtained in these irradiation experiments, which cover practically all the relevant cosmogenic nuclides, now allows a systematic description of the depth dependent nuclide production in small meteorites.

Table I Experimental Thin Target Cross Sections for the Production of Longlived Radionuclides and Stable Ne-Isotopes

Nuclide	Target	E_p [MeV]	σ [mb]
^{10}Be	O	600	1.52 ± 0.12
	Mg	600	1.03 ± 0.07
	Al	600	1.16 ± 0.07
	Si	600	0.63 ± 0.05
^{20}Ne	Mg	600	28.8 ± 0.2
	Al	600	23.7 ± 0.1
	Si	600	23.03 ± 0.05
^{21}Ne	Mg	600	28.6 ± 0.2
	Al	600	24.5 ± 0.2
	Si	600	20.7 ± 0.1
^{22}Ne (dir.)	Mg	600	12.5 ± 0.1
	Al	600	12.8 ± 0.1
	Si	600	7.6 ± 0.1
^{22}Ne (cum.)	Mg	600	44.5 ± 0.4
	Al	600	28.8 ± 0.2
	Si	600	26.0 ± 0.1
^{26}Al	Si	600	13.0 ± 0.8
	Fe	600	0.49 ± 0.02
	Ni	600	0.36 ± 0.02
^{41}Ca	Ti	41	7.1 ± 1.2
	Ti	81	18.2 ± 1.7
	Ni	98	0.08 ± 0.05
	Ni	140	0.29 ± 0.13
	Ni	184	0.94 ± 0.3

In order to unify the thick target approach used in these simulation experiments with the classical thin target approach [2,5] theoretical production rate depth profiles for the artificial meteorites were derived on the basis of Monte Carlo calculations of the nuclear spectra and of measured and calculated excitation functions. Fig.3 shows a comparison of experimental and theoretical data for the R=5cm artificial meteorite. Though there are still some discrepancies to be seen for low-energy neutron-induced products, the general agreement is excellent. Both the approaches promise a quality of the modelling of cosmic ray interaction with meteorites wich up to now has not been obtained.

1.2 Thin Target Cross Sections for the p-induced Production of Longlived Radionuclides and Stable Rare Gas Isotopes

An evaluation of existing thin target cross sections showed that there is sitll a considerable lack of data for the production of longlived radionuclides as well as of stable rare gas isotopes. Therefore, a systematic study of such nuclides in targets of earlier experiments has been started. First data on the production of ^{10}Be, ^{26}Al (long decay times), ^{41}Ca and of stable Ne isotopes are presented in Table I.

1.3 Theoretical Estimates of Cross Sections for Radionuclide Formation by High Energy Neutrons

A priori calculations of integral excitation functions for the production of radionuclides for n-energies between 2 and 190 MeV have been performed using the hybrid model of preequilibrium reactions [7,8]. The calculations cover now 20 target elements: Al, Mg, Si, Ca, Ti, V, Cr, Mn, Fe, Co, Ni, Cu, Y, Zr, Rh, Te, Ba, Lu, W and Au [9]. This consistent set of integral excitation functions for n-induced reactions is currently being tested via model calculations for radionuclide production in a variety of thick targets irradiated by high energy neutrons and protons.

References

[1] P.Englert, S.Theis, R.Michel, C.Tunis, R.K.Moniot, S.Vajda, T.H.Kruse, D.K.Pal, G.F.Herzog, Nucl. Instr. Methods Phys. Res. B5 (1984) 415

[2] R.Michel, P.Dragovitsch, P.Englert, F.Peiffer, R.Stück, S.Theis, F.Begemann, H.Weber, P.Signer, R.Wieler, D.Filges, P.Cloth, Nucl. Instr. Methods Phys. Res. 3 (1986) in press

[3] P.Dragovitsch, P.Englert, R.Michel, Proc. 19th International Cosmic Ray Conference, La Jolla, August 11-23 (1985) in press

[4] S.Theis, P.Englert, R.Michel, G.F.Herzog, T.H.Kruse, J.Klein, R.Middleton, Meteoritics (1985) in press

[5] R.Michel, Meteoritics (1985) in press

[6] S.Theis, P.Englert, R.Michel, D.Alymer, G.F.Herzog, T.H.Kruse, R.K.Moniot, C.Tunis, A.Jermakian, J.Klein, R.Middleton, Lun. Plan. Sci. XVII (1986) 887

[7] M.Blann, Phys. Rev. Lett. 27 (1971) 337

[8] M.Blann, J.Bisplinghoff, UCID-19614 (1982)

[9] F.Peiffer, R.Michel, KCK-N-SIG86 (1986), unpublished

INSTITUT FÜR KERNCHEMIE
UNIVERSITÄT MAINZ

1. Fission Yields and Isomeric Ratios

1.1 Nuclear Charge Distribution of Heavy Fission Products in the Reaction $^{233}U(n_{th},f)$ at Various Kinetic Energies of the Fission Fragments

C. Lietz, H.O. Denschlag, W. Ditz, U. Güttler,
B. Sohnius, P. Stumpf, H. Faust*

The mass separator LOHENGRIN [1] of the Institut Laue-Langevin (Grenoble) was used to measure the fractional independent yields in the following mass chains of the reaction $^{233}U(n_{th},f)$: 97, 99, 130, 132, 133, 134, 136, 137, 139, 141, and 144. The measurements were carried out at five values of the kinetic energy of the fission fragments. The targets used had a thickness ranging from 80 to 200 µg/cm^2 of $^{233}UO_2$ and were covered by a layer of Ta of 180 µg/cm^2 in thickness. After separation according to mass, kinetic energy and ionic charge state, the fission fragments left the separator through a thin window (6 µm of mylar foil). They were implanted into a transport tape and carried continuously in front of a shielded γ-ray detector. The γ-ray spectra were used to calculate [2] the independent yields of the single members of the decay chains. The yield values at the mean kinetic energy $\overline{E_{kin}}$ that are expected to agree with radiochemical yields are given in Table I; the values obtained for the other kinetic energies ($E_{kin}-\overline{E_{kin}} \cong \pm 3.5$ and ± 7 MeV) are given elsewhere [3].

---

* Institut Laue-Langevin, Grenoble, France

Table I Fractional independent (first chain members: fract. cumulative) Yields (YFI) in the Reaction $^{233}U(n_{th},f)$ at $\overline{E_{kin}}$. (Any independent contribution of chain members beyond the last chain member indicated has been neglected)

Nuclide	YFI	Error	Nuclide	YFI	Error
Sr-97	0.200	0.020	Te-136	0.088	0.005
Y-97	0.800	0.051	I-136	0.912	0.038
Y-99	0.234	0.013	Te-137	0.013	0.006
Zr-99	0.747	0.032	I-137	0.155	0.037
Nb-99	0.019	0.024	Xe-137	0.832	0.034
Sn-130	0.407	0.014	I-139	0.076	0.013
Sb-130	0.593	0.023	Xe-139	0.419	0.014
Sn-132	0.013	0.002	Cs-139	0.404	0.024
Sb-132	0.200	0.014	Ba-139	0.101	0.022
Te-132	0.788	0.023	Cs-141	0.585	0.038
Sb-133	0.179	0.012	Ba-141	0.415	0.058
Te-133	0.821	0.046	Ba-144	0.715	0.022
Te-134	0.632	0.025	La-144	0.285	0.029
I-134	0.368	0.034			

The new experimental results from this work may be compared with other yield measurements within the framework of Wahl's model [4]. The model parameters calculated using the yield values of this work are shown in Fig. 1.
They may be compared in the figure with values based on radiochemical yields and with values based on the yields of the light fission products in $^{233}U(n_{th},f)$. Except for a discrepancy at the highest kinetic energy, fair agreement exists for the parameters $^{140}\Delta Z$, σ, and EOZ. The parameter EON is not expected to show agreement of complementary fragments due to the emission of prompt neutrons. The parameter s, that describes the mass dependence of ΔZ is not shown in the figure, as it was constant around 0.02 ± 0.02.

A comparison of the energy dependence of $^{140}\Delta Z$ among heavy and light fragments indicates that the prompt neutron emission from fission fragments decreases by one unit when the kinetic energy of the light fragment increases by 15 MeV.

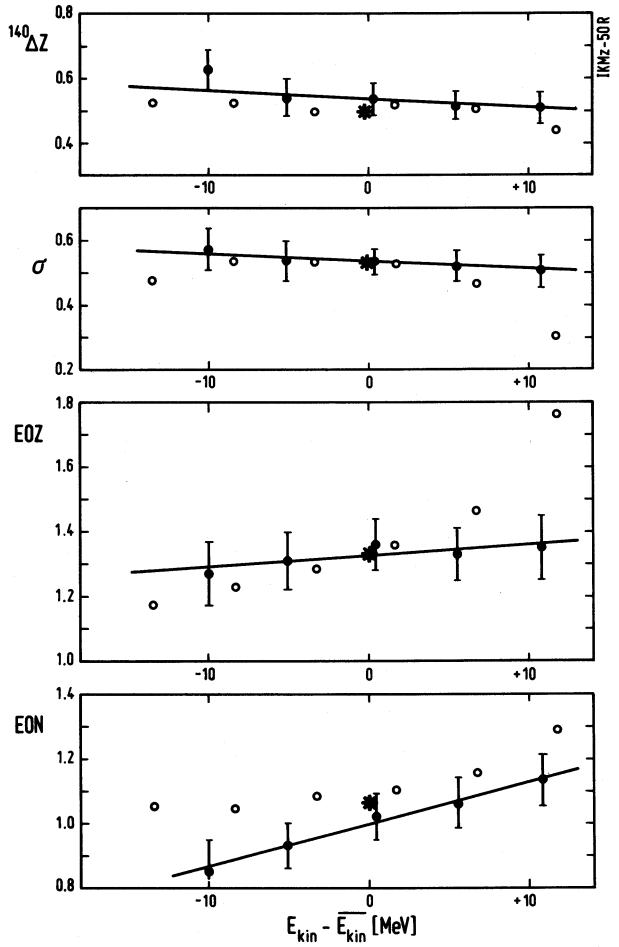

Fig. 1 Parameters of the fission yield model according to Wahl [4] calculated using yield values of this work (full points), radiochemical yield values (*) [4] and yield values of the light fission fragments (o) [5] at various kinetic energies of the light fragments (relative to the mean kinetic energy $\overline{E_{kin}}$).
($^{140}\Delta Z$: Charge displacement, $=Z_p - Z_{UCD}$ at A=140;
σ: width parameter of charge dispersion curve;
EOZ: even-odd factor for protons;
EON: even-odd factor for neutrons)

References

[1] E. Moll, H. Schrader, G. Siegert, M. Asghar, J.P. Bocquet, G. Bailleul, J.P. Gautheron, J. Greif, G.I. Crawford, C. Chauvin, H. Ewald, H. Wollnik, P. Armbruster, G. Fiebig, H. Lawin, and K. Sistemich, Nucl. Instr. Meth. 123 (1975) 615

[2] H.O. Denschlag, H. Braun, W. Faubel, G. Fischbach, H. Meixler, G. Paffrath, W. Pörsch, M. Weis, H. Schrader, G. Siegert, J. Blachot, Z.B. Alfassi, H.N. Erten, T. Izak-Biran, T. Tamai, A.C. Wahl, and K. Wolfsberg, in Physics and Chemistry of Fission (Proc. Symp. Jülich, 1979) IAEA,Vienna (1980), Vol. II, P. 153

[3] C. Lietz, Diplomarbeit, Mainz (1985) (in German)

[4] A.C. Wahl, J. Radioanalytical Chemistry, 55 (1980) 111

[5] U. Quade, Dissertation, München (1983) (in German)

1.2 Isomeric Ratios and Distribution of Angular Momentum in the Reaction $^{233}U(n_{th},f)$ at Various Kinetic Energies of the Fragments

C. Lietz, H.O. Denschlag, W. Ditz, U. Güttler, B. Sohnius, P. Stumpf, H. Faust*

The independent formation ratios of the isomeric states were measured for 7 nuclides at the mass separator LOHENGRIN [1] of the Institut Laue-Langevin (Grenoble) for the reaction $^{233}U(n_{th},f)$ at various kinetic energies of the fragments. The experimental conditions are given in paragraph 1.1 of

* Institut Laue-Langevin, Grenoble, France

this contribution. The fractions of high spin isomer relative to the total yield of the respective nuclide at the mean kinetic energy are given in Table I. The values measured at the mean kinetic energy are expected to agree with the corresponding radiochemical values. The values obtained for the other kinetic energies ($E_{kin}-\overline{E_{kin}} \cong \pm 3.5$ and $\pm$ 7 MeV) are given elsewhere [2].

Table I Fraction (F_H) of High Spin Isomer relative to the total Independent Yield of the respective Nuclide at the Mean Kinetic Energy of the Fragments in the Reaction $^{233}U(n_{th},f)$

Isomeric pair	F_H	Error
Y-97	0.695	$\pm$0.013
Sn-130	0.074	$\pm$0.008
Sb-130	0.467	$\pm$0.014
Sb-132	0.216	$\pm$0.036
Te-133	0.642	$\pm$0.018
I-134	0.285	$\pm$0.011
I-136	0.718	$\pm$0.012

The experimental isomeric ratios were used to calculate mean angular momenta ("J_{rms}") of the fission fragments using a simple statistical model formalism [3].
The results are plotted in Fig. 1 versus the kinetic energy of the fragments relative to their mean kinetic energy ($E_{kin}-\overline{E_{kin}}$) and may be compared there to the corresponding values in the fission of ^{235}U.
At the mean kinetic energies ($E_{kin}-\overline{E_{kin}}=0$) the angular momenta calculated for the two fission reactions agree quite well. Generally, they lie within the expected range of 5 to 8 $\hbar$ [3]. Only ^{130}Sn shows a lower angular momentum of about 3 $\hbar$ that may be due to the closure of the 50 proton shell in this even nucleus.

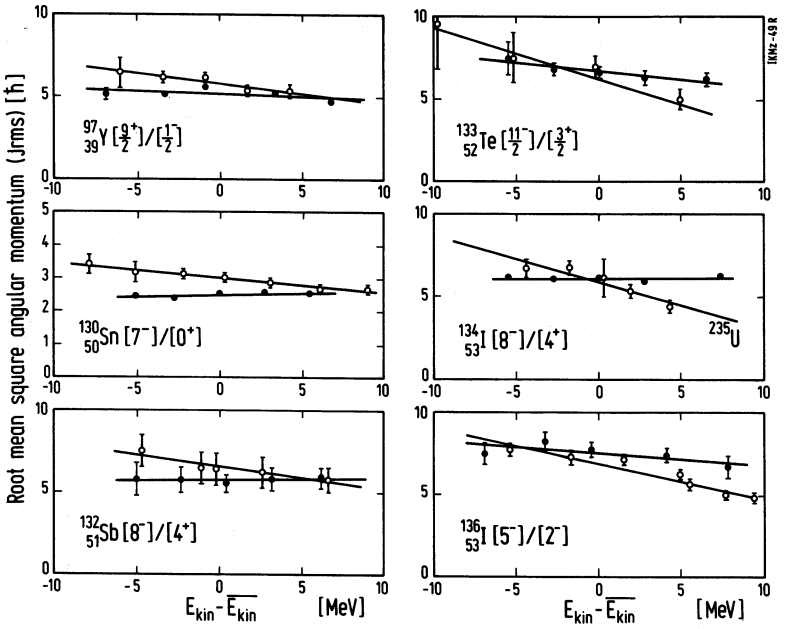

Fig. 1 Mean angular momentum calculated from experimental isomeric ratios of the isomeric pairs indicated at various kinetic energies of the fragments. Full points: $^{233}U(n_{th},f)$ (this work). Blank circles: $^{235}U(n_{th},f)$ (^{97}Y [4], ^{130}Sn [5], ^{132}Sb [6], ^{133}Te [6,7], ^{134}I [8], and ^{136}I [8]).

A remarkable difference between the two fission reactions exists for their energy dependence: ^{235}U shows a marked decrease of J_{rms} with increasing kinetic energy whereas ^{233}U presents a nearly constant behaviour.
Unfortunately, the ^{233}U-targets were somewhat inhomogenuous and, hence, had a less good energy resolution (e.g. FWHM 13.3 and 15.5 MeV for mass A=134 compared to 11 MeV for ^{235}U). A lower energy resolution, naturally, diminishes any energy dependence of J_{rms}. The observed difference between the two fission reactions can, however, not be explained by the different energy resolution of the targets. Therefore we deduce a different dynamical behaviour of the two compound nuclei that differ only by two neutrons.

References

[1] E. Moll, H. Schrader, G. Siegert, M. Asghar, J.P. Bocquet, G. Bailleul, J.P. Gautheron, J. Greif, G.I. Crawford, C. Chauvin, H. Ewald, H. Wollnik, P. Armbruster, G. Fiebig, H. Lawin, and K. Sistemich, Nucl. Instr. Meth. 123 (1975) 615

[2] C. Lietz, Diplomarbeit, Mainz (1985) (in German)

[3] D.G. Madland and T.R. England, Nucl. Science and Engineering, 64 (1977) 859

[4] St. Hörner, Diplomarbeit, Mainz (1985) (in German)

[5] W. Pörsch, Dissertation, Mainz in preparation (see also Institut Laue-Langevin, Annex to the Annual Report 1981, p. 29)

[6] H.O. Denschlag, H. Braun, W. Faubel, G. Fischbach, H. Meixler, G. Paffrath, W. Pörsch, M. Weis, H. Schrader, G. Siegert, J. Blachot, Z.B. Alfassi, H.N. Erten, T. Izak-Biran, T. Tamai, A.C. Wahl, and K. Wolfsberg, in Physics and Chemistry of Fission (Proc. Symp. Jülich, 1979) IAEA, Wien (1980), Vol. II, P. 153

[7] H. Braun, Dissertation, Mainz, (1983) (in German)

[8] W. Faubel, Dissertation, Mainz (1980) (in German)

INSTITUT FÜR STRAHLENPHYSIK
UNIVERSITÄT STUTTGART

1. Fast Polarized Neutron Scattering on ^{40}Ar, ^{40}Ca, Ni and Fe

G. Schreder, W. Grum, K.-W. Hoffmann, P.A. Owono*, H. Postner, G. Schleußner+, J.W. Hammer

In order to obtain systematic properties of nuclei, the program of polarized neutron scattering studies has been continued. The analysis of the calcium data obtained previously [1] led to the investigation of the neighbouring nucleus argon. For the argon experiment a cryogenic liquid sample contained in an extremely thin walled dewar has been used. At a neutron energy of 7.75 MeV analyzing power and differential cross section have been measured, the differential cross section relative to the hydrogen cross section. The scattering-contribution of the dewar walls has been determined experimentally. It was subtracted in the evaluation.

For the nickel and iron experiment very pure samples of natural isotopic abundance have been used. The evaluation of the experimental data is still in progress.

2. Optical Model Analysis and Data Reduction

G. Schreder, W. Grum, K.-W. Hoffmann, P.A. Owono, J.W. Hammer

Both nuclei ^{40}Ar and ^{40}Ca have been studied with a vibratonal coupled channels approach. The analysis of polarized data results in a substantial reduction of the freedom of the model parameters. For ^{40}Ca a strong octupole coupling had to be assumed to reproduce the experimental data. The angular distributions of differential cross section and analyzing power of ^{40}Ar are shown in Figs. 1 and 2 together with the coupled channel calculation results. For ^{40}Ca the differential cross section data of ENDF/B were used in the meantime, the evaluation of our data being not finished.

---

*Departement de Physique, Université de Yaounde, Kamerun
+Deceased

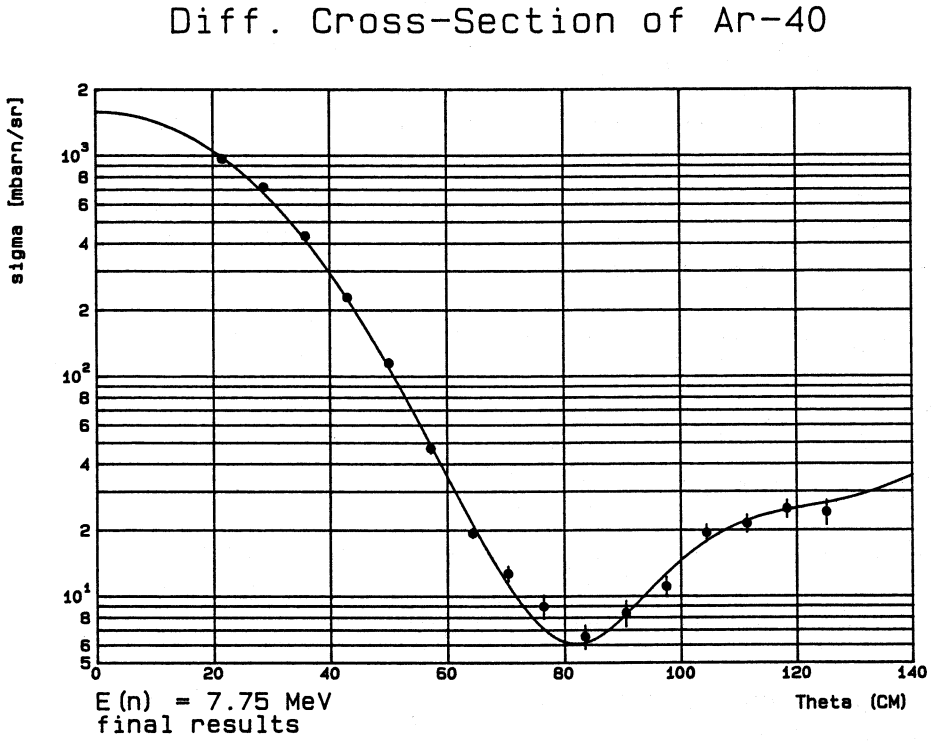

Fig. 1 Differential neutron cross section of ^{40}Ar at E_n = 7.75 MeV. Solid curve gives the cc-optical model fit.

The optical model parameters are given in Table I.

Table I (all potentials in MeV, all lengths in fm)

	v_r	r_v	a_v	W_I	r_w	a_w	v_{so}	r_{so}	a_{so}	β_2	β_3
Ar	52.61	1.17	0.73	2.19	1.26	0.58	6.1	1.02	0.58	0.30	----
Ca	51.31	1.22	0.69	3.72	1.22	0.58	5.87	0.81	0.68	0.18	0.49

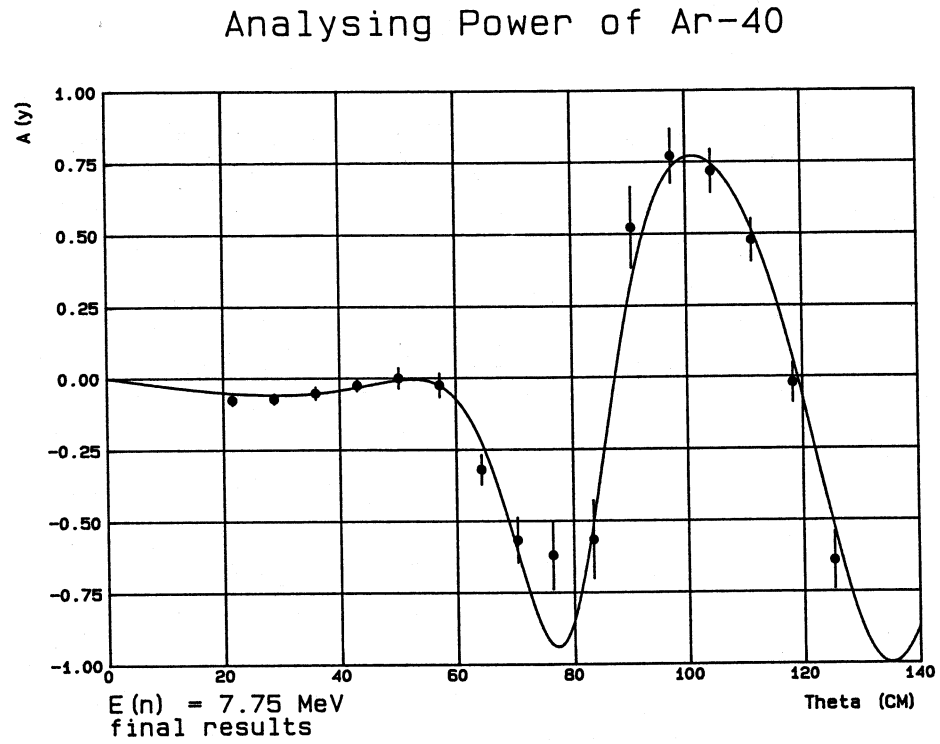

Fig. 2 Analyzing power of ^{40}Ar for 7.75 MeV neutrons. Solid curve shows the cc-optical model results with parameter set of Table I.

The optical model analysis for the heavy nuclei (^{238}U, ^{232}Th, $^{n.}Pb$, ^{208}Pb, ^{206}Pb, ^{209}Bi, W, Ta) is in progress and will be reported when finished. The previous ^{12}C scattering data have been reevaluated using improved codes and the results are given in [2].

In collaboration with von Geramb, Hamburg, some calculations have been performed using a microscopic nuclear model. While for light nuclei the behaviour of analyzing power and differential cross section could be described satisfactorily, for the heavier nuclei large discrepancies exist and will be subject of further investigations.

[1] H. Postner, Diplomarbeit, Stuttgart 1982

[2] J.W. Hammer, G. Bulski, W. Grum, W. Kratschmer, H. Postner, G. Schleußner, Nucl. Instr. and Meth. A 244 (1986) 455

Reaktorstation Garching
Fachbereich Physik
Technische Universität München

1. Coherent Neutron Scattering Lengths and Total Cross Sections

1.1 Neutron Scattering Lengths and Cross Sections of the Barium Isotopes

L.Koester, K.Knopf, W.Waschkowski

Coherent neutron scattering lengths and total cross sections have been measured for barium compounds and on isotopically enriched samples for neutron energies from 0.5 meV up to 132 eV using different techniques. From the experimental data the following quantities were obtained:

- the coherent scattering lengths (in fm) of Ba (5.07±0.03) and of the isotopes with mass numbers 130 (-3.6±0.6); 132 (7.8±0.3); 134 (5.7±0.1); 135 (4.66±0.10); 136 (4.90±0.08); 137 (6.82±0.10); and 138 (4.83±0.08).
- the absorption cross sections σ_γ(at 0.025 eV) in barn:

of Ba(1.1±0.1) and of the isotopes: 130 (30±5); 136 (0.68±0.17); 137 (3.6±0.2); and 138 (0.27±0.14).
- zero-energy scattering cross sections for Ba and the isotopes 136, 137 and 138.

On the basis of these data, the isotopic- and spin-incoherent cross sections and the (s)-resonance contributions to the coherent scattering lengths have been determined and discussed.

Published in Z.Phys.A 322 (1985) 105

1.2 Interactions of Slow Neutrons with Nuclides of Antimony, Tellurium and Iodine

L.Koester, K.Knopf, W.Waschkowski

Coherent neutron scattering lengths and total cross sections have been measured on samples of ordinary Sb,Te,I and on isotopically enriched compounds. From the experimental data for neutron energies of 0.57 meV, 1.26 eV and 5.2 eV the following data were obtained:
- the coherent scattering lengths (in fm) of the bound atoms Sb (5.57±0.03); ^{121}Sb(5.71±0.06), ^{123}Sb(5.38±0.07); Te(5.80±0.03) and for its isotopes of the mass number 122(3.8±0.2); 123(-0.05±0.25-i·0.100); 124(7.95±0.10); 125(5.01±0.08); 126(5.55±0.07); 128(5.88±0.07); 130(6.01±0.07),
- the thermal absorption cross sections (in barn) for Sb(4.91±0.05); ^{121}Sb(5.77±0.12); ^{123}Sb(3.8±0.2); Te(4.05±0.05) and I(6.15±0.06).

The combination of the measured values of scattering lengths and -cross sections resulted in data for coherent and incoherent cross sections. Taking account of resonance data a complete set of spin state- and resonance scattering lengths has been obtained and discussed.

Submitted to Z.Phys.A (Oct. 1985)

1.3 Neutron Scattering Lengths of the Isotopes of Thulium, Ytterbium and Lutetium

L.Koester, K.Knopf

Coherent neutron scattering lengths and total cross sections have been measured on samples of ordinary Tm, Yb and Lu and on isotopically enriched compounds. From the experimental data for 0.57 meV neutron energy the following data were obtained:
- the coherent scattering lengths (in fm) of the bound atoms ^{169}Tm (7.07±0.03); ^{170}Yb(6.8±0.1); ^{171}Yb(9.7±0.1); ^{172}Yb(9.5±0.1); ^{173}Yb(9.56±0.10); ^{174}Yb(19.2±0.1); ^{176}Yb(8.7±0.1); Yb(12.41±0.03); ^{175}Lu(7.28±0.09); ^{176}Lu(6.3±0.2) and Lu(7.23±0.03);
- the thermal absorption cross sections (in barn) for ^{169}Tm(100±2); Yb(34.8±0.8) and Lu(74±2).

In combination with the resonance parameters the measured coherent scattering lengths allowed the determination of potential scattering radii R' which are of particular interest for the permanently deformed and deformable nuclei in the rare-earth region.

submitted to Z.Phys.A (Nov. 1985)

2. Fundamental Properties

2.1 Neutron Scattering Lengths and Neutron-Electron Interaction

L.Koester, W.Waschkowski, A.Klüver

After a discussion of the electromagnetic contributions to the neutron-nucleus scattering length we report on methods for the determination of scattering lengths and on precision techniques which allow the separation of the electromagnetic from the nuclear scattering length. We used this effect for a new determination of the effective neutron-electron scattering length $-(1.32\pm0.04) \cdot 10^{-3}$ fm and for the separation of the electric polarization scattering of the neutron. At the present status of the experiment we obtain polarization scattering lengths from experiments of $(3\pm4) \cdot 10^{-3}$ fm^3, in agreement with theoretical predictions.

To be published in Physica / North Holland (Dec. 1985)

INSTITUT FÜR KERNCHEMIE
PHILIPPS UNIVERSITÄT MARBURG

1. Gamma-Ray Catalog

W. Westmeier

Quantitative information on gamma rays from the decay of radioactive nuclides is required in many areas of nuclear science as well as related fields. We have therefore produced a compilation of decay properties of all known radionuclides, with the main emphasis on energies and absolute intensities of the gamma rays. A first printed version of this catalog was issued in 1979, and a second edition, including references through June 1982, was completed in 1983. The second version contains information on 2526 nuclides and isomers with a total of more than 47.000 gamma rays and X-rays, the information on X-rays accompanying radioactive decay being a newly introduced feature. The catalog is presented in two parts: In Part I gamma rays are listed in order of increasing energy for the purpose of identification of unknown gamma lines. In Part II complete data sets for each nuclide are listed in order of mass number A and nuclear charge Z of the nuclides. This part also contains additional information, references, and comments in case of any discrepancies.
The second version of the catalog was published in "Atomic Data and Nuclear Data Tables", Volume 29, Nos. 1,2 (1983).
At present, a third and completely updated version of the catalog is in preparation where the literature cutoff date is estimated to be about June 1987.

2. Alpha-Particle Catalog

W. Westmeier , A. Merklin

A table of alpha-decay properties of all known alpha-emitting nuclides, which includes data on alpha energies, intensities, and the abundances of the alpha branch, has been compiled. The table is laid out in a manner similar to the Gamma-Ray Catalog and it has been published in "Physik Daten / Physics Data", Nr. 29-1, Fachinformationszentrum Energie Physik Mathematik GmbH, Karlsruhe, 1985, ISSN 0344-8401.

Both tables are compiled and updated under the auspices of the Fachinformationszentrum Energie Physik Mathematik GmbH (FIZ) in Karlsruhe.

PHYSIKALISCH-TECHNISCHE BUNDESANSTALT
BRAUNSCHWEIG

1. Cross Sections

1.1 Differential Cross Section of $^{16}O(n,n)^{16}O$ at 10.17 MeV

G. Börker, R. Böttger, H.J. Brede, H. Klein, W. Mannhart,
B.R.L. Siebert

The scattering of 10.17 MeV neutrons produced via the $D(d,n)^3He$ reaction was investigated at the PTB TOF-facility using H_2O, BeO, Al_2O_3 and SiO_2 samples. The differential cross section of the non-oxygen contents of the samples was separately measured on Be, Al, and Si samples. Finite geometry and multiple scattering effects were taken into account by extensive Monte Carlo calculations. The smallest uncertainty (3 ... 7 %) for the differential cross section on oxygen could be achieved using the H_2O sample, taking special care in the subtraction of the contributions due to the Al container enclosing the water and due to the surrounding air. The result is shown in Fig. 1 including a comparison with ENDF/B-V data and a TUNL measurement at 10.21 MeV [1]. In agreement with the TUNL analysis the total elastic cross section is found to be 15 percent lower than predicted by ENDF/B-V.

The analysis of measurements at additional 8 energies between 6 MeV and 15 MeV is in progress.

1.2 Cross Section Determination of the Reactions $^{12}C(n,\alpha_o)^9Be$ and $^{12}C(n,n'3\alpha)$ between E_n = 7.6 and 10.2 MeV

H.J. Brede, G. Dietze, H. Klein, H. Schölermann

The neutron induced reactions on carbon $^{12}C(n,\alpha_o)^9Be$ and $^{12}C(n,n'3\alpha)$ have been studied for incident neutron energies between 7.6 and 10.2 MeV. The cross sections were determined by comparing measured and calculated response spectra of an NE 213 scintillation detector [2, 3].

The monoenergetic neutrons were selected using the TOF facility at the PTB cyclotron. The scintillation detector with a known content of carbon and hydrogen nuclei simultaneously served as a carbon target, an α-particle detector and a neutron

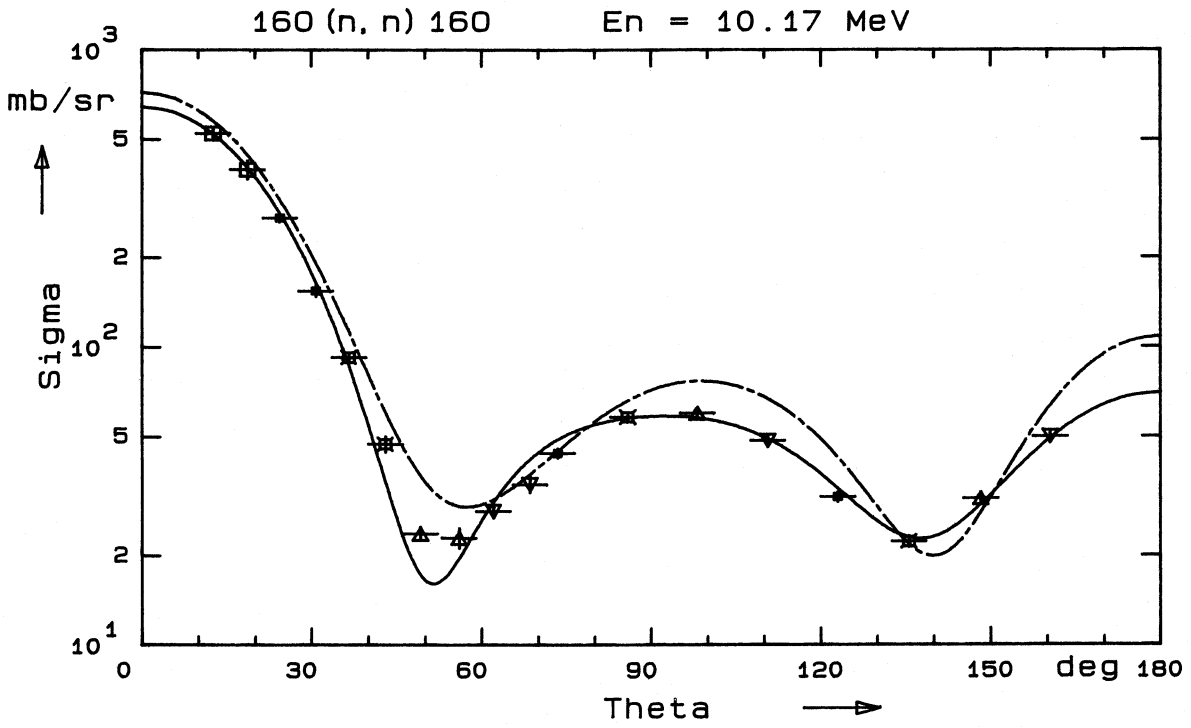

Fig. 1 The scattering cross section for 10.17 MeV neutrons on oxygen is shown versus the effective lab. angle. The present PTB data are compared with a recent TUNL measurement (straight line) and ENDF/B-V data (dashed-dotted line).

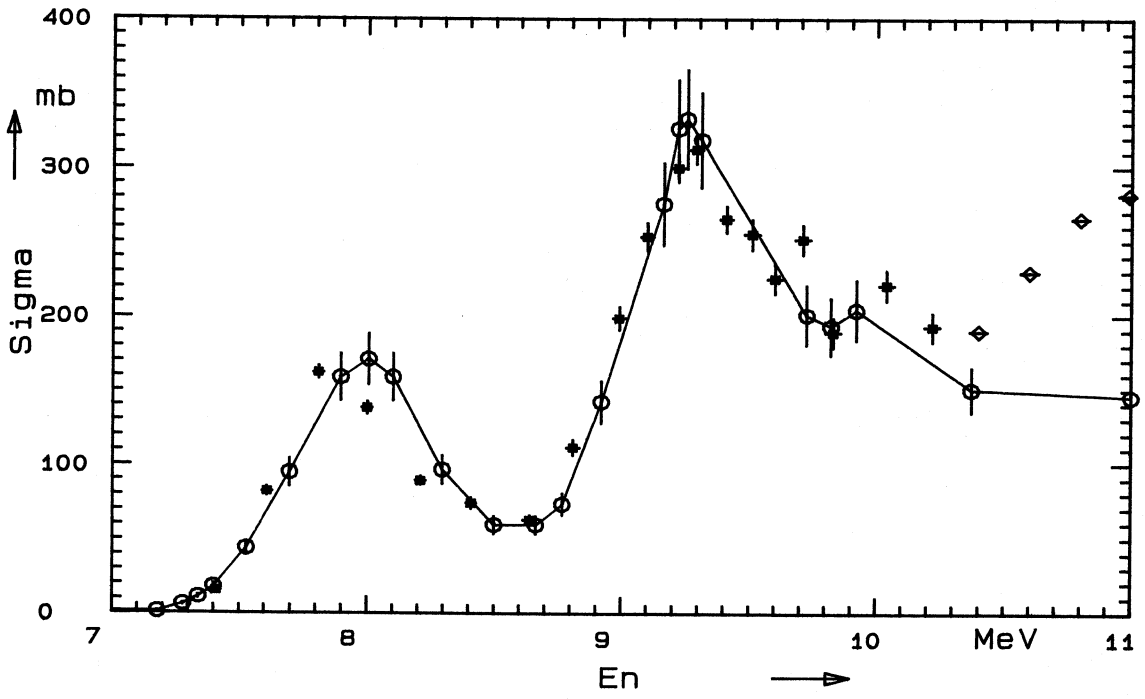

Fig. 2 Cross section data for the $^{12}C(n,\alpha_0)^{9}Be$ and $^{12}C(n,n'3\alpha)$ reactions as a function of the neutron energy (ϕ ENDF/B-V data [6]; $\diamond$ data of Kudo and Dietze [5]; * present measurement)

fluence monitor. The neutron response function of the NE 213 scintillation detector was calculated by means of the Monte Carlo code NRESP5 [4]. The fraction of the response spectrum induced by α-particles could be separated. The α-particle events referring to the $^{12}C(n,\alpha_o)^{9}Be$ or the $^{12}C(n,n'3\alpha)$ reaction channels can be classified if the shape of the angular distribution of the $^{12}C(n,\alpha_o)^{9}Be$ reaction is known [5].

Fig. 2 shows the sum of the $^{12}C(n,\alpha_o)^{9}Be$ and the $^{12}C(n,n'3\alpha)$ cross section values extracted by the comparison between the experiment and the simulation with the Monte Carlo code NRESP5 as a function of neutron energy.

There are some discrepancies in the absolute value of the cross section for E_n near 8 MeV and especially in the energy range above 9.7 MeV between the ENDF/B-V (open circles) [6] and our data (squares). The data points above E_n = 10.2 MeV (rhombs) are from the analysis of Kudo and Dietze [5].

1.3 Cross Sections for Fast Neutron Induced Reactions on Carbon

Br. Antolkovic[+], G. Dietze, H. Klein

Fast neutron induced reactions on carbon were studied in the energy range of 11.5 MeV $\leq E_n \leq$ 19 MeV. In a twin experiment an NE 213 liquid scintillator and nuclear emulsions were simultaneously used as carbon target and 4 π charged particle detector.

The measured scintillator response for monoenergetic neutrons is compared with Monte Carlo simulations [4]. This enables the sum of the kinematically allowed reactions on carbon to be directly related to the n-p reference cross section. In steps of 0.5 MeV (0.2 MeV between 14.0 MeV and 15.0 MeV) determined with an uncertainty of about ± 4 % this total reaction cross section shows deviations from evaluated data ENDF/B-V [6] up to ± 15 %.

The nuclear emulsions irradiated in the same neutron field were scanned for three-pronged alpha stars, this method being exclusively sensitive to the breakup reaction C(n,n'3α) [7]. Besides the total cross section determined with uncertainties of 5 ... 15 %, details of the various sequential decay chains such as branching ratios and angular distributions can be extracted.

[+] Ruder Boskovic Institute, Zagreb, Yugoslavia

This information and reliable angular distribution parameters for the remaining (or their inverse) reactions are needed for the MC simulations before partial cross sections can be extracted from the scintillator response.

References

[1] S.G. Glendinning, S. El-Kadi, C.E. Nelson, F.O. Purser C.R. Gould and L.W. Seagondollar, Nucl. Sci. Eng. 82, (1982) 393

[2] G. Dietze, H.J. Brede, H. Klein and H. Schölermann, Nuclear Data for Science and Technology, Proc. of the Int. Conf. in Antwerp, ed. K.H. Böckhoff, Reichel Publ. Comp., Dordrecht, (1983) p. 484

[3] Progress Report Neutron Dosimetry, (1982/83) p. 28

[4] G. Dietze and H. Klein, PTB-Report ND-22 (1982)

[5] K. Kudo and G. Dietze, Bull. Electrotechn. Lab., Japan, 49 (1985) 23

[6] Nuclear Data File ENDF/B-V, Brookhaven National Laboratory

[7] Br. Antolkovic, I. Slaus, D. Plenkovic, P. Macq , J.P. Meulders, Nucl. Phys. A394 (1983) 87

2. Radionuclide Data

2.1 Half-Lives

H. Schrader, K.F. Walz

The half-lives of the radionuclides ^{24}Na, ^{169}Yb and ^{195}Au were determined by following the decay of the radioactive substance with a pressurized $4\pi\gamma$ ionization chamber. A source consisted of 2 ml radioactive solution in a sealed glass ampoule. The sources were examined for impurities by germanium detector measurements. The stability of the chamber was checked by measurements of a radium reference source at the beginning and at the end of each measuring cycle. The data have been evaluated by least squares fits. Details of the data evaluation and results have been published [1]. The results for the three radionuclides are summarized in Table I. The given uncertainties (in parentheses) correspond to one standard deviation and include systematic uncertainties. The measuring period t is given as ratio to the half-life $T_{1/2}$.

[1] K.F. Walz, K. Debertin and H. Schrader; Int.J.Appl.Rad. Isot. 34 (1983) 1191

Table I Half-Lives

Nuclide	$t/T_{1/2}$	$T_{1/2}$
^{24}Na	9	0.62323 (12) d
^{169}Yb	5	32.032 (19) d
^{195}Au	3	186.12 (10) d

2.2 Photon Emission Probabilities

U. Schötzig

Photon emission probabilities p of ^{89}Sr, ^{109}Cd, ^{147}Pm and ^{204}Tl were determined by using sources of known activity and calibrated Ge(Li) and high purity Ge spectrometers. The results are summarized in the Table II, uncertainties given in parentheses correspond to one standard deviation.

Table II Photon Emission Probabilities

Nuclide	Energy in keV	p
^{89}Sr	909	$9.61(13).10^{-5}$
^{109}Cd	88	0.0368(7)
^{147}Pm	121	$2.64(6).10^{-5}$
^{204}Tl	$69\text{-}83(K_{\alpha}+K_{\beta})$	0.01486(19)

FACHINFORMATIONSZENTRUM ENERGIE, PHYSIK, MATHEMATIK GMBH

Status Report

H. Behrens, P. Luksch, H.W. Müller

1. Recent Compilations

The following new issues were published in the series Physics Data:

21-1 (1985) Bibliography of Gas Phase Electron Diffraction Supplement 1980-82
E. Herde, E. Maier, B. Mez-Starck, R. Mutter, U. Seiter, C. Spreter, I. Hargittai, D.G. Watson, A. Lohr, G.J. Selz

29-1 (1985) Catalog of Alpha Particles from Radioactive Decay
W. Westermeier, A. Merklin

16-5 (1986) Frameworks for "Intermetallic Phases" with structures in Space Groups of the 4-Stem of I4/mmm
E. Hellner, W.B. Pearson

2. The Evaluated Nuclear Structure Data File (ENSDF)

The FIZ Karlsruhe is participating in the International Nuclear Structure and Decay Data Network. The FIZ is responsible for the evaluation of data in the mass range from A=81 to 100.

In 1985 the mass chains A=81,94, and 97 have been published , the mass chains A=83 and 99 have been finished and will be published in 1986. At the moment, the evaluation of A=82 and A=93 is in progress.

The online retrievable file ENSDF has been updated in March and in November. Since in a general clean-up the whole database has been formally improved, the new file had to be loaded in total. The size of the file has increased by about 23%. Presently, the file contains 9,430 data sets, each describing a special experiment. In total 597,919 80-byte records are needed to store the information.

The radioactive decay data for the MEDLIST file have been derived from the ENSDF file. The file contains at the moment data of 2,097 decay branches.

The bibliographic data base Nuclear Structure References (NSR) has been updated 3 times. 4,200 references have been added. The current file contains 100,826 references.

APPENDIX I

Addresses of Contributing Laboratories

Institut für Kernphysik II
Director: Prof. Dr. A. Citron
Senior reporter: Dr. S. Cierjacks
Kernforschungszentrum Karlsruhe
Postfach 3640
7500 Karlsruhe

Institut für Kernphysik III
Director: Prof. Dr. G. Schatz
Senior reporter: Dr. F. Käppeler
Kernforschungszentrum Karlsruhe
Postfach 3640
7500 Karlsruhe

Institut für Neutronenphysik und Reaktortechnik
Director: Prof. Dr. G. Kessler
Senior reporter: Dr. F.H. Fröhner
Kernforschungszentrum Karlsruhe
Postfach 3640
7500 Karlsruhe

Institut für Chemie (1): Nuklearchemie
Director: Prof. Dr. G. Stöcklin
Senior reporter: Dr. S.M. Qaim
Kernforschungsanlage Jülich
Postfach 1913
5170 Jülich

Institut für Reine und Angewandte Kernphysik
Director: Prof. Dr. K.O. Thielheim
Senior reporter: Dr. H.-G. Priesmeyer
Universität Kiel, Geesthacht
Reaktorstr. 1
2054 Geesthacht/Tesperhude

I. Institut für Experimentalphysik
Senior reporter: Prof. Dr. W. Scobel
Universität Hamburg
Luruper Chaussee 149
2000 Hamburg 50

Institut für Biochemie, Abteilung Nuklearchemie
Head: Prof. Dr. G. Stöcklin
Senior reporter: Dr. U. Herpers
Universität zu Köln
Zülpicher Str. 47
5000 Köln

Institut für Kernchemie
Director: Prof. Dr. G. Herrmann
Senior reporter: Prof. Dr. H.O. Denschlag
Universität Mainz
Fritz-Strassmann-Weg 2
6500 Mainz

Institut für Strahlenphysik
Director: Prof. Dr. K.W. Hoffmann
Senior reporter: Dr. J.W. Hammer
Universität Stuttgart
Allmandring 3
7000 Stuttgart 80

Fachbereich Physik der
Technischen Universität München
Abteilung E14, Forschungsreaktor
Head and senior reporter: Prof. Dr. L. Köster
8046 Garching/München

Institut für Kernchemie
Senior reporter: Prof. Dr. P. Patzelt
Philipps-Universität Marburg
Lahnberge
3550 Marburg/Lahn

Physikalisch-Technische Bundesanstalt
Abteilung 6, Atomphysik
Director: Prof. Dr. S. Wagner
Bundesallee 100
3300 Braunschweig

Fachinformationszentrum Energie, Physik, Mathematik
Directors: Drs. W. Rittberger, E.-O. Schulze
Senior reporter: Dr. H. Behrens
Kernforschungszentrum
7514 Eggenstein-Leopoldshafen 2

APPENDIX II

CINDA Type Index

Prepared by H. Behrens and G. Schust
FIZ Energie, Physik, Mathematik, Karlsruhe

ELEMENTS	A	QUANTITY	TYPE	ENERGY MIN	ENERGY MAX	DOCUMENTATION REF	VOL	PAGE	DATE	LAB	COMMENTS
H	001	TOTAL	EXPT-ABST	24+4		NEANDC(E)-272U	686		KIG		VOL.5.P.19.PRIESMEYER. TOF EXPT
LI	007	N,N TRITON	EXPT-ABST	80+6	11+7	NEANDC(E)-272U	686		JUL		VOL.5.P.16.WOELFLE+ NO DATA GIVEN
LI	007	N,TRITON	EXPT-ABST	FAST		NEANDC(E)-272U	686		JUL		VOL.5.P.16.WOELFLE+ SIG, NO DATA GIV
BE	009	N,TRITON	EXPT-ABST	FAST		NEANDC(E)-272U	686		JUL		VOL.5.P.16.WOELFLE+ SIG, NO DATA GIV
B	010	N,TRITON	EXPT-ABST	FAST		NEANDC(E)-272U	686		JUL		VOL.5.P.16.WOELFLE+ SIG, NO DATA GIV
B	010	N,TRITON	EXPT-ABST	80+6	11+7	NEANDC(E)-272U	686		JUL		VOL.5.P.16.WOELFLE+ NO DATA GIVEN
C		N,PROTON	EXPT-ABST	12+7	19+7	NEANDC(E)-272U	686		GER		VOL.5.P.48.ANTOLKOVIC+ TOT SIG,NDG
C	012	N,ALPHA	EXPT-ABST	76+6		NEANDC(E)-272U	686		GER		VOL.5.P.46.BREDE+ SIG,GRAPH
C	012	N,N ALPHA	EXPT-ABST	10+7		NEANDC(E)-272U	686		GER		VOL.5.P.46.BREDE+ (N,N3A)SIG,GRAPH
O	016	DIFF ELASTIC	EXPT-ABST	10+7		NEANDC(E)-272U	686		GER		VOL.5.P.46.BOERKER+ ANG DIST,GRAPH
MG		N,GAMMA	THEO-ABST	20+6	19+8	NEANDC(E)-272U	686		KLN		VOL.5.P.32.DRAGOVITSCH+ EXCIT FN,NDG
AL		N,GAMMA	THEO-ABST	20+6	19+8	NEANDC(E)-272U	686		KLN		VOL.5.P.32.DRAGOVITSCH+ EXCIT FN,NDG
SI		N,GAMMA	THEO-ABST	20+6	19+8	NEANDC(E)-272U	686		KLN		VOL.5.P.32.DRAGOVITSCH+ EXCIT FN,NDG
AR	040	N,GAMMA	EXPT-ABST	23+4		NEANDC(E)-272U	686		KFK		VOL.5.P.5.BEER+ MAXW AVERAGED SIG
AR	040	POLARIZATION	EXPT-ABST	78+6		NEANDC(E)-272U	686		THS		VOL.5.P.40.SCHREDER+ SIG ANALYS.POW
AR	040	POLARIZATION	THEO-ABST	78+6		NEANDC(E)-272U	686		THS		VOL.5.P.40.SCHREDER+ OPTMDL CALC
CA		N,GAMMA	THEO-ABST	20+6	19+8	NEANDC(E)-272U	686		KLN		VOL.5.P.32.DRAGOVITSCH+ EXCIT FN,NDG
CA	040	POLARIZATION	EXPT-ABST	78+6		NEANDC(E)-272U	686		THS		VOL.5.P.40.SCHREDER+ NO DATA GIVEN
CA	040	POLARIZATION	THEO-ABST	78+6		NEANDC(E)-272U	686		THS		VOL.5.P.40.SCHREDER+ OPTMDL,NO DATA
TI		N,GAMMA	THEO-ABST	20+6	19+8	NEANDC(E)-272U	686		KLN		VOL.5.P.32.DRAGOVITSCH+ EXCIT FN,NDG
V		N,GAMMA	THEO-ABST	20+6	19+8	NEANDC(E)-272U	686		KLN		VOL.5.P.32.DRAGOVITSCH+ EXCIT FN,NDG
V	051	N,N ALPHA	EXPT-ABST	15+7		NEANDC(E)-272U	686		JUL		VOL.5.P.16.WOELFLE+ ACTIVATION SIG
CR		N,GAMMA	THEO-ABST	20+6	19+8	NEANDC(E)-272U	686		KLN		VOL.5.P.32.DRAGOVITSCH+ EXCIT FN,NDG
MN		N,GAMMA	THEO-ABST	20+6	19+8	NEANDC(E)-272U	686		KLN		VOL.5.P.32.DRAGOVITSCH+ EXCIT FN,NDG
FE		N,GAMMA	THEO-ABST	20+6	19+8	NEANDC(E)-272U	686		KLN		VOL.5.P.32.DRAGOVITSCH+ EXCIT FN,NDG
FE		POLARIZATION	EXPT-ABST	78+6		NEANDC(E)-272U	686		THS		VOL.5.P.40.SCHREDER+ NO DATA GIVEN
FE	056	RESON PARAMS	EXPT-ABST	01+3		NEANDC(E)-272U	686		KFK		VOL.5.P.6.CORVI+ FROM CAPT EXPT
CO		N,GAMMA	THEO-ABST	20+6	19+8	NEANDC(E)-272U	686		KLN		VOL.5.P.32.DRAGOVITSCH+ EXCIT FN,NDG
NI		N,GAMMA	THEO-ABST	20+6	19+8	NEANDC(E)-272U	686		KLN		VOL.5.P.32.DRAGOVITSCH+ EXCIT FN,NDG
NI		POLARIZATION	EXPT-ABST	78+6		NEANDC(E)-272U	686		THS		VOL.5.P.40.SCHREDER+ NO DATA GIVEN
CU		N,GAMMA	THEO-ABST	20+6	19+8	NEANDC(E)-272U	686		KLN		VOL.5.P.32.DRAGOVITSCH+ EXCIT FN,NDG
SE	078	N,GAMMA	EXPT-ABST	PILE		NEANDC(E)-272U	686		KFK		VOL.5.P.7.KLAY+ BETA-DECAY OF SE79M
KR	084	N,GAMMA	EXPT-ABST	54+4		NEANDC(E)-272U	686		KFK		VOL.5.P.8.KAEPPELER+ KR85M ISOMERY
Y		N,GAMMA	THEO-ABST	20+6	19+8	NEANDC(E)-272U	686		KLN		VOL.5.P.32.DRAGOVITSCH+ EXCIT FN,NDG
ZR		N,GAMMA	THEO-ABST	20+6	19+8	NEANDC(E)-272U	686		KLN		VOL.5.P.32.DRAGOVITSCH+ EXCIT FN,NDG
NB	093	N,HELIUM3	EXPT-ABST	60+6	10+7	NEANDC(E)-272U	686		JUL		VOL.5.P.14.QAIM+ EXCITATION FUNCTION
MO	092	N,N ALPHA	EXPT-ABST	15+7		NEANDC(E)-272U	686		JUL		VOL.5.P.16.WOELFLE+ ACTIVATION SIG
RH		N,GAMMA	THEO-ABST	20+6	19+8	NEANDC(E)-272U	686		KLN		VOL.5.P.32.DRAGOVITSCH+ EXCIT FN,NDG
IN	115	N,N ALPHA	EXPT-ABST	15+7		NEANDC(E)-272U	686		JUL		VOL.5.P.16.WOELFLE+ ACTIVATION SIG
SB		THERMAL SCAT	EXPT-ABST	57-4	52+0	NEANDC(E)-272U	686		MUN		VOL.5.P.43.KOESTER+ SCAT LENGTH,SIG
SB	121	THERMAL SCAT	EXPT-ABST	57-4	52+0	NEANDC(E)-272U	686		MUN		VOL.5.P.43.KOESTER+ SCAT LENGTH,SIG
SB	123	THERMAL SCAT	EXPT-ABST	57-4	52+0	NEANDC(E)-272U	686		MUN		VOL.5.P.43.KOESTER+ SCAT LENGTH,SIG

ELEMENTS	A	QUANTITY	TYPE	ENERGY MIN	ENERGY MAX	DOCUMENTATION REF	VOL	PAGE	DATE	LAB	COMMENTS
TE		N,GAMMA	THEO-ABST	20+6	19+8	NEANDC(E)-272U	686			KLN	VOL.5.P.32.DRAGOVITSCH+ EXCIT FN,NDG
TE		THERMAL SCAT	EXPT-ABST	57-4	52+0	NEANDC(E)-272U	686			MUN	VOL.5.P.43.KOESTER+ SCAT LENGTH,SIG
TE	122	THERMAL SCAT	EXPT-ABST	57-4	52+0	NEANDC(E)-272U	686			MUN	VOL.5.P.43.KOESTER+ SCAT LENGTH
TE	123	THERMAL SCAT	EXPT-ABST	57-4	52+0	NEANDC(E)-272U	686			MUN	VOL.5.P.43.KOESTER+ SCAT LENGTH
TE	124	THERMAL SCAT	EXPT-ABST	57-4	52+0	NEANDC(E)-272U	686			MUN	VOL.5.P.43.KOESTER+ SCAT LENGTH
TE	125	THERMAL SCAT	EXPT-ABST	57-4	52+0	NEANDC(E)-272U	686			MUN	VOL.5.P.43.KOESTER+ SCAT LENGTH
TE	126	THERMAL SCAT	EXPT-ABST	57-4	52+0	NEANDC(E)-272U	686			MUN	VOL.5.P.43.KOESTER+ SCAT LENGTH
TE	128	THERMAL SCAT	EXPT-ABST	57-4	52+0	NEANDC(E)-272U	686			MUN	VOL.5.P.43.KOESTER+ SCAT LENGTH
TE	130	THERMAL SCAT	EXPT-ABST	57-4	52+0	NEANDC(E)-272U	686			MUN	VOL.5.P.43.KOESTER+ SCAT LENGTH
I		THERMAL SCAT	EXPT-ABST	57-4	52+0	NEANDC(E)-272U	686			MUN	VOL.5.P.43.KOESTER+ SCAT LENGTH,SIG
BA		N,GAMMA	THEO-ABST	20+6	19+8	NEANDC(E)-272U	686			KLN	VOL.5.P.32.DRAGOVITSCH+ EXCIT FN,NDG
BA		THERMAL SCAT	EXPT-ABST	50-4	13+2	NEANDC(E)-272U	686			MUN	VOL.5.P.43.KOESTER+ SCAT LENGTH,SIG
BA	130	THERMAL SCAT	EXPT-ABST	50-4	13+2	NEANDC(E)-272U	686			MUN	VOL.5.P.43.KOESTER+ SCAT LENGTH,SIG
BA	132	THERMAL SCAT	EXPT-ABST	50-4	13+2	NEANDC(E)-272U	686			MUN	VOL.5.P.43.KOESTER+ SCAT LENGTH
BA	134	THERMAL SCAT	EXPT-ABST	50-4	13+2	NEANDC(E)-272U	686			MUN	VOL.5.P.43.KOESTER+ SCAT LENGTH
BA	135	THERMAL SCAT	EXPT-ABST	50-4	13+2	NEANDC(E)-272U	686			MUN	VOL.5.P.43.KOESTER+ SCAT LENGTH
BA	136	THERMAL SCAT	EXPT-ABST	50-4	13+2	NEANDC(E)-272U	686			MUN	VOL.5.P.43.KOESTER+ SCAT LENGTH,SIG
BA	137	THERMAL SCAT	EXPT-ABST	50-4	13+2	NEANDC(E)-272U	686			MUN	VOL.5.P.43.KOESTER+ SCAT LENGTH,SIG
BA	138	THERMAL SCAT	EXPT-ABST	50-4	13+2	NEANDC(E)-272U	686			MUN	VOL.5.P.43.KOESTER+ SCAT LENGTH,SIG
LA	139	N,GAMMA	EXPT-ABST	23+4		NEANDC(E)-272U	686			KFK	VOL.5.P.8.BEER. MAXWELL AVERAGED SIG
DY	156	N,GAMMA	EXPT-ABST	23+4		NEANDC(E)-272U	686			KFK	VOL.5.P.10.BEER. MAXW AVERAGED SIG
HO	165	N,N ALPHA	EXPT-ABST	15+7		NEANDC(E)-272U	686			JUL	VOL.5.P.16.WOELFLE+ ACTIVATION SIG
TM	169	THERMAL SCAT	EXPT-ABST	57-4		NEANDC(E)-272U	686			MUN	VOL.5.P.44.KOESTER+ SCAT LENGTH,SIG
YB		THERMAL SCAT	EXPT-ABST	57-4		NEANDC(E)-272U	686			MUN	VOL.5.P.44.KOESTER+ SCAT LENGTH,SIG
YB	170	THERMAL SCAT	EXPT-ABST	57-4		NEANDC(E)-272U	686			MUN	VOL.5.P.44.KOESTER+ SCAT LENGTH
YB	171	THERMAL SCAT	EXPT-ABST	57-4		NEANDC(E)-272U	686			MUN	VOL.5.P.44.KOESTER+ SCAT LENGTH
YB	172	THERMAL SCAT	EXPT-ABST	57-4		NEANDC(E)-272U	686			MUN	VOL.5.P.44.KOESTER+ SCAT LENGTH
YB	173	THERMAL SCAT	EXPT-ABST	57-4		NEANDC(E)-272U	686			MUN	VOL.5.P.44.KOESTER+ SCAT LENGTH
YB	174	THERMAL SCAT	EXPT-ABST	57-4		NEANDC(E)-272U	686			MUN	VOL.5.P.44.KOESTER+ SCAT LENGTH
YB	176	N,N ALPHA	EXPT-ABST	15+7		NEANDC(E)-272U	686			JUL	VOL.5.P.16.WOELFLE+ ACTIVATION SIG
YB	176	THERMAL SCAT	EXPT-ABST	57-4		NEANDC(E)-272U	686			MUN	VOL.5.P.44.KOESTER+ SCAT LENGTH
LU		THERMAL SCAT	EXPT-ABST	57-4		NEANDC(E)-272U	686			MUN	VOL.5.P.44.KOESTER+ SCAT LENGTH,SIG
LU	175	THERMAL SCAT	EXPT-ABST	57-4		NEANDC(E)-272U	686			MUN	VOL.5.P.44.KOESTER+ SCAT LENGTH
LU	176	THERMAL SCAT	EXPT-ABST	57-4		NEANDC(E)-272U	686			MUN	VOL.5.P.44.KOESTER+ SCAT LENGTH
TA	181	N,TRITON	EXPT-ABST	14+7	19+7	NEANDC(E)-272U	686			JUL	VOL.5.P.14.QAIM+ EXCITATION FUNCTION
PT	194	N,GAMMA	EXPT-ABST	23+4		NEANDC(E)-272U	686			KFK	VOL.5.P.10.BEER. MAXW AVERAGED SIG
PT	196	N,GAMMA	EXPT-ABST	23+4		NEANDC(E)-272U	686			KFK	VOL.5.P.10.BEER. MAXW AVERAGED SIG
PT	198	N,GAMMA	EXPT-ABST	23+4		NEANDC(E)-272U	686			KFK	VOL.5.P.10.BEER. MAXW AVERAGED SIG
U	233	FRAG CHARGE	EXPT-ABST	PILE		NEANDC(E)-272U	686			MNZ	VOL.5.P.33.LIETZ+ FRACT YIELDS
U	233	FRAG CHARGE	EXPT-ABST	PILE		NEANDC(E)-272U	686			MNZ	VOL.5.P.36.LIETZ+ ANG MOMENTUM DISTR
NP	237	FRAG SPECTRA	EXPT-ABST	FAST		NEANDC(E)-272U	686			KFK	VOL.5.P.11.NAQVI+ KIN ENERGIES,NDG